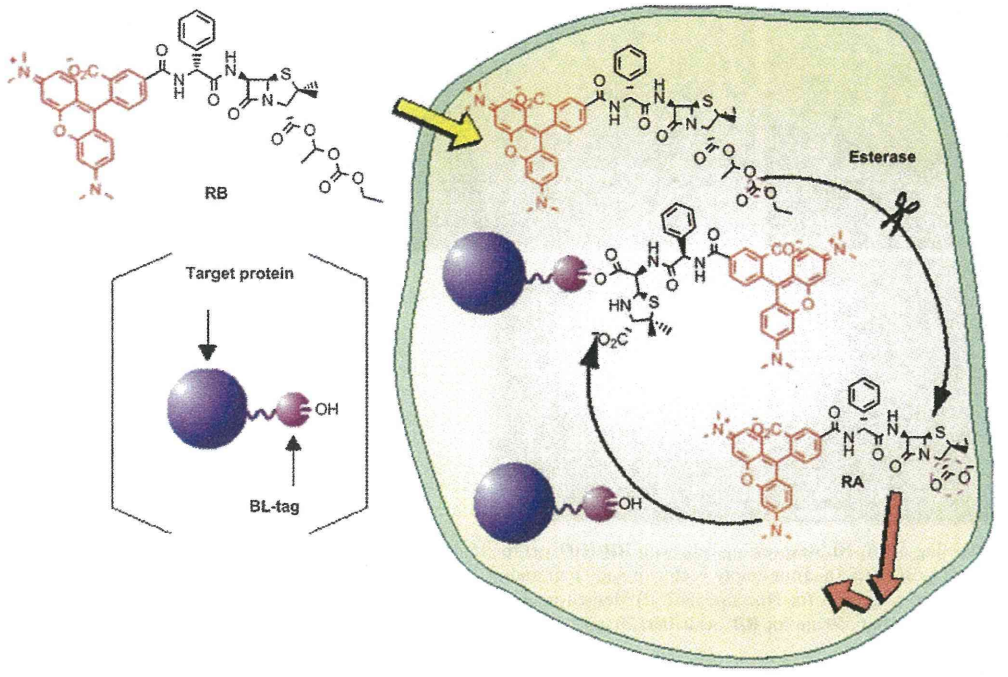

Scheme 2. Labeling mechanism of the intracellular BL-tag fusion proteins by **RB**.

form of BL proteins, the bacterial signal sequence was removed and replaced by an initiator methionine (cytoplasmic-BL).[16] To enhance expression levels, a consensus sequence for optimal translation efficiency in eukaryotes[17] was added adjacent to the initiator codon. Furthermore, to facilitate the detection of the fluorescent label, we designed BL-NLS, which is a nuclear localized BL protein, by fusing the BL-tag to three consecutive simian virus 40 (SV40) large T antigen nuclear localization sequences (NLS).[18] The intracellular expression of cytoplasmic-BL and BL-NLS were confirmed by western blot analysis (see the Supporting Information, Figure S3). Lysates of cells transfected with cytoplasmic-BL plasmids were probed with an anti-β-lactamase antibody, which revealed one major band with a molecular weight of about 25 kDa, corresponding to a cytoplasmic-BL fusion protein (see the Supporting Information, Figure S3 A; lane 1). A single band was also detected in cells transfected with BL-NLS (see the Supporting Information, Figure S3 A; lane 2). This band appeared in a slightly higher position than that of cytoplasmic-BL, which is consistent with the increase in molecular weight due to the fusion of three consecutive NLS.

HEK293T cells transfected with a vector expressing cytoplasmic-BL or BL-NLS were incubated with **RB** at a lower concentration (100 nM) than labeling probes in reported methods.[3,4] After the washing step, red fluorescence was uniformly observed in cytoplasmic-BL-expressing cells (Figure 1). In BL-NLS-expressing cells, strong red fluorescence was detected at the cell center (Figure 2a), and the nuclear localization of the fluorescently labeled proteins was confirmed by co-staining with Hoechst 33342, which binds

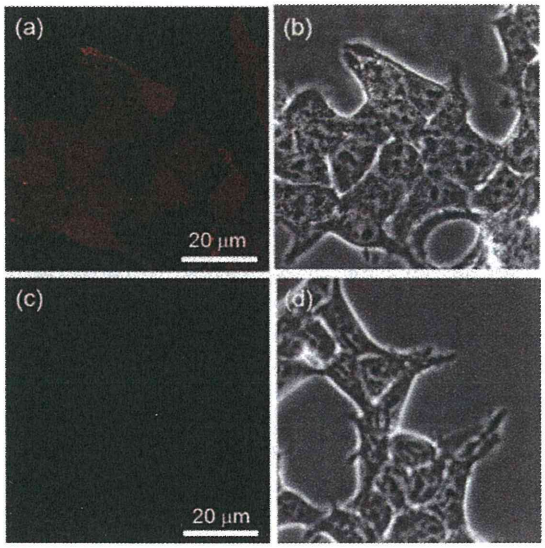

Figure 1. Specific labeling of cytoplasmic-BL-expressing cells with **RB** (100 nM) for 15 min. HEK293T cells were transfected with a plasmid encoding (a) and cytoplasmic-BL (b) or empty vector (c and d). a) and c) Fluorescence images. b) and d) Phase contrast images. For fluorescence microscopic images, the cells were excited at 559 nm. Scale bar: 20 μm.

to DNA in the nucleus (Figure 2d). The merged fluorescence image indicates the specific labeling of BL-NLS by **RB**. Nonspecific accumulation of **RB** in **RB**-treated cells was not observed, despite the fact that rhodamine-based fluorescent probes often show nonspecific accumulation in organelles such as mitochondria owing to their positive charge

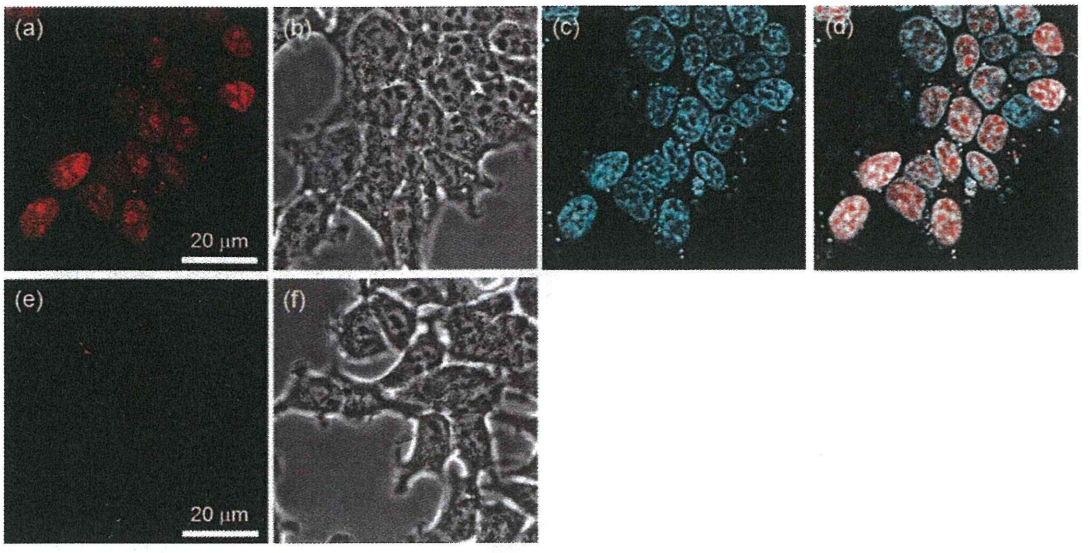

Figure 2. Specific labeling of BL-NLS-expressing cells with **RB** (100 nM) for 15 min and co-stained with Hoechst33342. HEK293T cells were transfected with a plasmid encoding BL-NLS (a–d) or empty vector (e and f). a) and e) Fluorescence images of a channel for **RB**. b) and f) Phase contrast images. c) Fluorescence images of a channel for Hoechst33342. d) Merged image of a) and c). For fluorescence microscopic images, the cells were excited at 405 nm for Hoechst33342 and at 559 nm for **RB**. Scale bar: 20 μm.

and hydrophobicity. Rhodamine derivatives are therefore often used as probes for mitochondria.[19] When cells expressing BL-NLS were incubated with high concentrations of **RA** (5 μM), no staining of the cell nuclei was observed (see the Supporting Information, Figure S4). The intracellular labeling experiments suggested that the cell permeability of the labeling probe would be largely improved by introducing a bacampicillin structure into the probe design.

Subsequently, labeling of BL-NLS fusion proteins with **FB** or **FB-DA** was attempted using the same concentration (100 nM) as for **RB**. Incubation of cells expressing BL-NLS with **FB** did not show fluorescence in the nuclei (Figure 3a and 3b). On the other hand, nuclei of cells treated with **FB-DA** showed strong green fluorescent signals (Figure 3c and 3d). These results indicate that the cell permeability of BL-tag labeling probes depends on not only the carboxy group of the β-lactam substrates but also on the structure of the fluorophores. **FB-DA** showed sufficient cell permeability because the anionic groups of the fluorescein moiety are wholly acetylated.

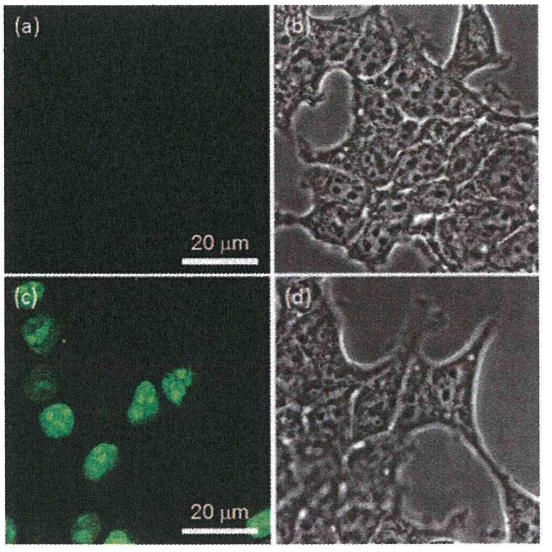

Figure 3. Specific labeling of BL-NLS-expressing cells with **FB** (100 nM) (a and b) or **FB-DA** (100 nM) (c and d) for 15 min. HEK293T cells were transfected with a plasmid encoding BL-NLS. a) and c) Fluorescence images. b) and d) Phase contrast images. For fluorescence microscopic images, the cells were excited at 473 nm. Scale bar: 20 μm.

Simultaneous and discriminative labeling of BL-tag fusion proteins localized at the cell surface and intracellular regions: A unique application of prodrug-based labeling technology, namely the simultaneous discriminative labeling of BL-tag fusion proteins localized at the cell surface and intracellular regions, was demonstrated (Scheme 3). The ability to discriminate between membrane proteins and intracellular proteins in the same cell is critical for the understanding of protein trafficking.[20] Protein labeling methods use cell-permeable probes for intracellular protein labeling that are also recognized by the target proteins on the cell surface. Therefore, to perform discriminative labeling with a single tag, the extracellular target proteins need to be blocked with cell-impermeable probes to allow specific labeling of intracellular proteins by cell-permeable probes.

In the present experiments, the tag recognition ability of bacampicillin-based labeling probes was expected to be largely suppressed before esterase-mediated hydrolysis. Because esterified benzylpenicillin is a very poor substrate for class A β-lactamases,[9] a negatively charged substituent on the substrate is essential for the recognition by β-lacta-

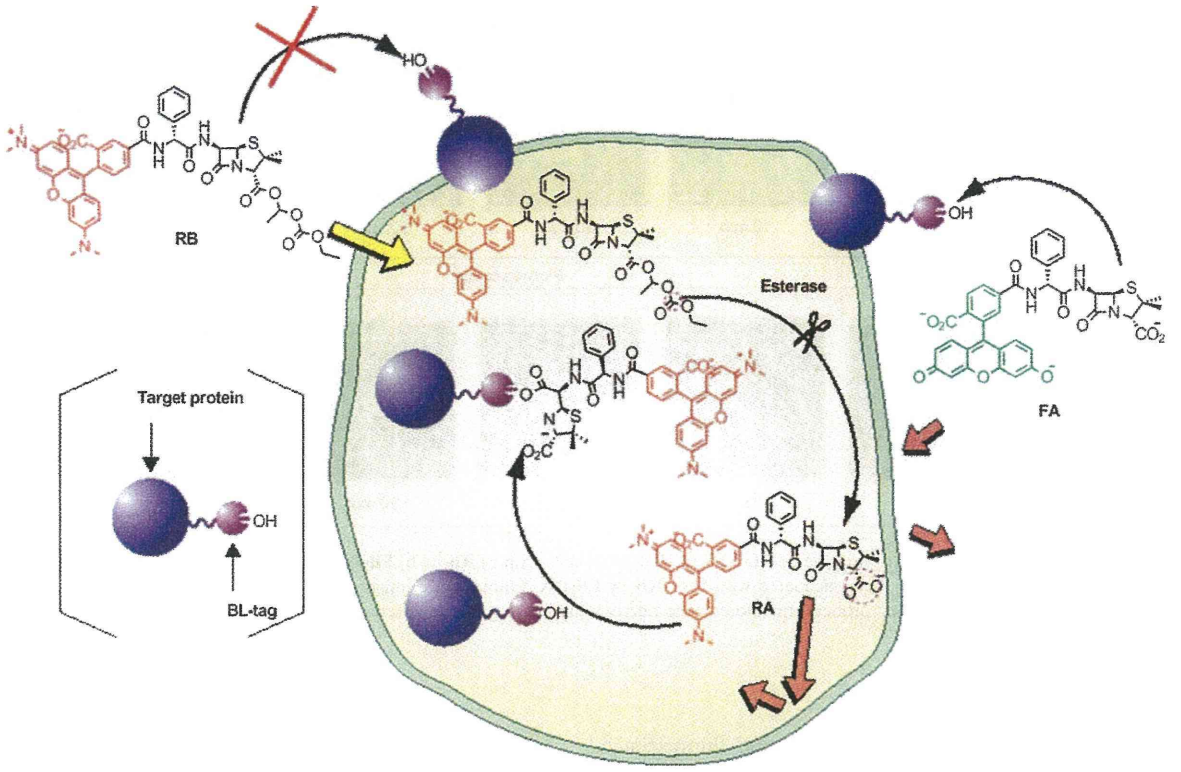

Scheme 3. Simultaneous discriminative labeling mechanism of the intracellular and cell surface BL-tag fusion proteins by using **RB** and **FA**.

mase.[21] Purified BL-tag proteins (10 μM) were incubated with **RA** (12 μM), **FA** (12 μM), or **RB** (100 μM) in 100 mM HEPES buffer (pH 7.4) at 25 °C. The reaction mixtures were sampled at various time points and analyzed by SDS-PAGE (Figure S5 in Supporting Information). The fluorescently labeled proteins were detected by irradiating the gels with UV light. A time course of fluorescent band signals was used to evaluate the labeling reaction rates of the three probes with the BL-tag protein. The in vitro reaction of the BL-tag protein with **RB** was significantly slower than that of **FA** and **RA**, even in the presence of excess amount of substrates. Hence, ampicillin-based probes such as **RA** and **FA** preferentially react with extracellular BL-tag fusion proteins compared with bacampicilin-based probes such as **RB** and **FB-DA**.

The two kinds of fusion proteins, BL-NLS and BL-EGFR, were used for the simultaneous labeling experiment. BL-EGFR is the result of the fusion of the BL-tag with epidermal growth factor receptor (EGFR). We previously succeeded in labeling cell surface BL-EGFR with ampicillin-based labeling probes.[6b] HEK293T cells co-expressing BL-NLS and BL-EGFR were incubated with **RB** (100 nM) and **FA** (100 nM) simultaneously, and then washed before imaging with a confocal fluorescence microscope. As shown in Figure 4, green fluorescence corresponding to **FA** was observed along the plasma membranes and red fluorescence corresponding to **RB** was observed in the nuclei. The present results demonstrate the successful selective labeling of intracellular and membrane proteins with two different colored fluorophores by using the same tag.

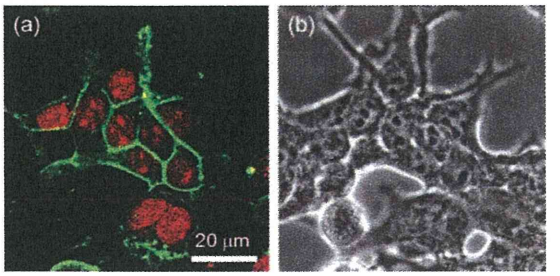

Figure 4. Simultaneous labeling of BL-tag fusion proteins localized at the cell membrane and nucleus. HEK293T cells were transfected with two kinds of plasmids encoding BL-NLS and BL-EGFR, and labeled with **RB** (100 nM) and **FA** (100 nM) for 15 min. a) Fluorescence merged image of labeled cells. b) Phase contrast image. For fluorescence microscopic images, the cells were excited at 473 nm for **FA** and 559 nm for **RB**. Scale bar: 20 μm.

Fluorescence labeling of BL-NLS proteins without washing procedure: Finally, time-lapse imaging of BL-NLS fusion proteins, fluorescently labeled with **RB** or **FB-DA**, was carried out using low probe concentrations. Surprisingly, a decrease in the concentration of the probe to 5 nM resulted in the detection of specific protein labeling within a 30 min period without a washing procedure (Figure 5, and Supplementary movies S1 and S2 in Supporting Information). This

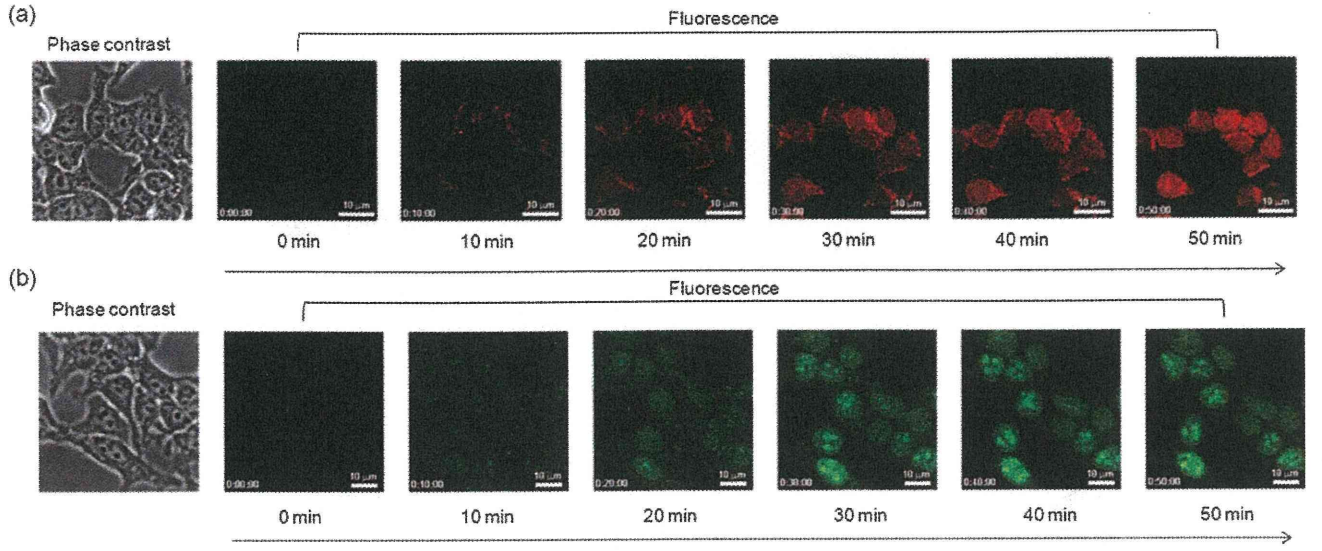

Figure 5. No-wash time-lapse (0–50 min) imaging of BL-NLS in HEK293T cells with a) **RB** or b) **FB-DA**. The cells were transfected with a plasmid encoding BL-NLS. The transfected cells were incubated with 5 nM **RB** or **FB-DA**. Fluorescence images were captured every 1 min without any washing procedure after the addition of labeling probes. For fluorescence microscopic images, the cells were excited at 473 nm for **FB-DA** and 559 nm for **RB**. Scale bar: 10 μm.

effect is due to the low levels of background fluorescence from the unreacted labeling probes present at reduced probe concentrations. In addition, the prodrug-based probes efficiently permeated cell membranes and accumulated inside cells owing to the rapid regeneration of anionic groups by esterases. This increased the local concentration of active BL-tag labeling probes, thus enabling efficient and specific visualization of intracellular BL-tag without a required washing step. Labeling of intracellular proteins at such a low probe concentration is difficult using existing labeling methods because of low membrane permeability of the labeling probes and low reaction efficiency with target proteins.

Conclusion

We have developed the cell-permeable labeling probes **RB** and **FB-DA** by using the clinical prodrug antibiotic bacampicillin. The probes rapidly recover their labeling activity through hydrolysis by esterases present in cells, and specifically label intracellular BL-tag fusion proteins localized in the cytosol and nucleus at nanomolar probe concentrations. Because prodrug-based probes are activated only inside cells, intracellular and cell surface BL-tag fusion proteins were discriminatively labeled by a simple combination of cell-permeable and impermeable probes. Moreover, owing to the quick entry and intracellular accumulation of the probe, very low probe concentrations are required, which enables the detection of fluorescently labeled proteins such as BL-NLS without a washing step to remove unreacted probes.

Existing labeling methods use complicated labeling procedures for discriminative labeling. Therefore, this technology would be quite useful for real-time spatial analysis of protein dynamics such as translocation from the cytosol to the extracellular membrane region. The prodrug-based probe design strategy would enable the control of various probe functions by in cell or in vivo enzyme activities. In addition, the present combination of BL-tag technology and prodrug-based labeling probes is important for real-time investigation of the localization and trafficking of target proteins in living cells, for which protein labeling without the removal of excess probe by washing is required. Because prodrugs in clinical applications have been well characterized regarding ADME (absorption, delivery, metabolism, and excretion) properties, this strategy could also be applied for the design of in vivo imaging probes.

Experimental Section

Construction of the cytoplasmic-BL plasmid: (see the Supporting Information, Scheme S2a) A DNA fragment of BL containing a termination codon was amplified from the BL-EGFR[6b] plasmid by the polymerase chain reaction (PCR) using the following primers containing the Kozak sequence[17] (forward primer: 5′-GTAATCGCTAGCGCCGCCATGGCCCACCCAGA-3′, subforward primer: 5′-GTAATCGCTAGCGCC-3′, reverse primer: 5′-GCGACTAAGCTTTTACCAATGCTTAATCA GTG-3′, subreverse primer: 5′-GCGACTAAGCTTTTACCA-3′). The amplified insert was digested with NheI and HindIII, and ligated in-frame to a similarly digested pcDNA 3.1(+) vector.

Construction of the BL-NLS plasmid: (see the Supporting Information, Scheme S2b). A DNA fragment of BL without a termination codon was amplified from the BL-EGFR plasmid by PCR using the following primers containing the Kozak sequence (forward primer: 5′-GTAATCGC-

TAGCGCCGCCATGGCCCACCCAGA-3′, subforward primer: 5′-GTAATCGCTAGCGCC-3′, reverse primer: 5′-GCGACTAAGCTTC-CAATGCTTAATCAGTGAG-3′, subreverse primer: 5′-GCGAC-TAAGCTTCCAAT-3′). The amplified insert was digested with NheI and HindIII, and ligated in-frame to a similarly digested pcDNA 3.1(+) vector (pcDNA 3.1(+)-BL-without terminator codon). The pcDNA 3.1(+)-BL-without terminator codon vector was digested with HindIII and BamHI, and ligated in-frame to a similarly digested NLS oligo DNA. The NLS oligo DNA was amplified from a purchased oligo nucleotide template (5′-AATCGAAAGCTTGGAGGATCTGGA GATCT-GATCCAAAAAAGAAGAGAAAGGTAGATCCAAAAAAGAA-GAG-3′ and 5′-ATCGCAGGATCCTTATACCTTTCTCTTTTTCTTAG-GATCAACCTTCCTCTTCTTTTTTGGATCTACC-3′: Gene design Inc.) using the following primers (forward primer: 5′-AATC-GAAGCTTGGAGG-3′, reverse primer: 5′-GCGACTAAGCTTC-CAATGCTTA ATCAGTGAG-3′).

Fluorometric analysis: A slit width of 2.5 nm was used for both excitation and emission, and the photomultiplier voltage was 700 V. All fluorescent probes were dissolved in DMSO to obtain 10 mM stock solutions and these solutions were diluted to the desired final concentrations with an appropriate aqueous buffer. The relative fluorescence quantum yields of the compounds were obtained by comparing the area under the emission spectrum of the sample with that of a 0.5 μM EtOH solution of rhodamine B (fluorescence quantum yield of 0.97 when excited at 545 nm),[22] and a NaOH (100 mM) aqueous solution of fluorescein (quantum efficiency of 0.85 when excited at 492 nm).[23]

Fluorescence Microscopy: Fluorescence microscopic images were recorded using a confocal laser scanning microscope (Olympus, FLUOVIEW FV10i) equipped with a 60× lens. The emission filter sets used were Olympus BA490–540 for **FA**, **FB**, and **FB-DA**, and BA570–620 for **RA** and **RB**.

HPLC analysis: HPLC analyses were performed with an Inertsil ODS-3 (4.6 mm×250 mm) column (GL Sciences Inc.) using an HPLC system composed of a pump (PU-2080, JASCO) and a detector (MD-2010 and FP-2020, JASCO). Preparative HPLC was performed with an Inertsil ODS-3 (10.0 mm×250 mm) column (GL Sciences Inc.) using an HPLC system with a pump (PU-2087, JASCO) and a detector (UV-2075, JASCO).

Esterase treatment assay of RB: The esterase reaction solution (5 units mL^{-1}) was prepared in HEPES buffer (100 mM, pH 7.4). **RB** stock solution (1 mM in DMSO) was added to the esterase reaction solution (final concentration: 10 μM). The reaction mixture was incubated at 25°C for 10 min, and the reaction product was analyzed by reversed-phase HPLC.

Labeling of BL-NLS with cell-permeable probes: HEK293T cells maintained in a poly-L-lysine-coated glass-bottomed dish (Matsunami) with DMEM (Invitrogen) containing FBS (10%) at 37°C under CO_2 (5%) were transfected with a plasmid coding for BL-NLS, using Lipofectamine 2000 (Invitrogen), and the cells were incubated at 37°C for 24 h. The cells were then washed once with Hank's balanced salt solution (HBSS) and incubated with **FB**, **FB-DA**, and **RB** (100 nM) at 37°C for 15 min. The cell nuclei were co-stained with Hoechst 33342 (200 ng mL^{-1}). After washing of unreacted probes with HBSS, the fluorescence images of the cells in HBSS were captured with appropriate filter sets. For labeling experiments of BL-NLS-expressing cells, the labeled cells were observed soon after the washing step.

Labeling of cytoplasmic-BL with cell-permeable probes: A plasmid coding for cytoplasmic-BL was transfected into HEK293T cells as described above. The cells were washed once with HBSS and incubated with **RB** (100 nM) at 37°C for 15 min. Cells were imaged in HBSS with the appropriate filter sets 60 min after washing of unreacted probes by HBSS.

Simultaneous labeling of BL-tag fusion proteins at the cell membrane and nucleus: Two plasmids coding for BL-EGFR and BL-NLS were transfected into HEK293T cells as described above. The cells were then washed once with HBSS, and incubated with **RB** (100 nM) and **FA** (100 nM) at 37°C for 15 min. After removal of unreacted probes with HBSS, the fluorescence images of cells in HBSS were captured with the appropriate filter sets.

No-wash time-lapse imaging of BL-NLS labeling by RB or FB-DA: A plasmid coding for BL-NLS was transfected into HEK293T cells as described above. The cells were then washed once with HBSS and incubated with **RB** or **FB-DA** (5 nM) at 37°C. The fluorescence images of cells were captured at 1 min intervals in HBSS without a washing step. The captured images were analyzed by ImageJ software.

Western blot analysis of cytoplasmic-BL and BL-NLS expressed in HEK293T cells: HEK293T cells were transfected with cytoplasmic-BL or BL-NLS using Lipofectamine 2000 and the cells were incubated at 37°C for 24 h. The cells were then washed once with PBS (−) and lysed with 200 μL of 1× SDS gel loading buffer (50 mM Tris-HCl buffer (pH 6.8), SDS (1.3%), glycerol (10%), and mercaptoethanol (5%)). After scraping, the lysates were boiled at 95°C for 3 min. Samples were electrophoresed in a 15% SDS-polyacrylamide gel, and transferred to polyvinylidene difluoride (PVDF) membranes for western blot analysis. The membranes were blocked with tris-buffered saline tween-20 (TBST, Tween 20 (0.01%), NaCl (138 mM), Tris (20 mM), pH 7.6) containing 5% skimmed milk for 1 h at RT. Then, the anti-β-lactamase (1:5000 dilution), or anti-β-actin (1:5000 dilution) antibody was added to each membrane. After incubation for 16 h at 4°C with shaking, the membranes were washed three times with TBST buffer, incubated with horseradish peroxidase-linked secondary antibody, washed with TBST buffer, and visualized using enhanced chemiluminescence (ECL) western blotting detection reagents.

Estimation of the reaction rate of BL-tag with labeling probes: Purified BL-tag (10 μM)[6a] was added to a solution of a series of labeling probes (**RA** (12 μM), **FA** (12 μM), and **RB** (100 μM)) in HEPES buffer (100 mM, pH 7.4) at RT. For the analysis of the binding reaction rate, the reaction mixture was sampled at various time points. Samples were mixed with 2× sample buffer (Tris-HCl buffer (100 mM, pH 6.8), SDS (2.5%), glycerol (20%), and mercaptoethanol (10%)) and subjected to SDS-PAGE. After electrophoresis, the fluorescently labeled proteins were detected with AE6931FXCF Printgraph (ATTO).

Acknowledgements

This work was supported in part by the Grant-in-Aid for Scientific Research from the Ministry of Education, Culture, Sports, Science and Technology of Japan (MEXT), by the Grant-in-Aid from the Ministry of Health, Labor and Welfare of Japan (MHLW), and by the New Energy and Industrial Technology Development Organization of Japan (NEDO). K.K. thanks support from the Takeda Science Foundation. K.K. and S.M. thank support from the Asahi Glass Foundation. S.W. acknowledges support from a Global COE Fellowship of Osaka University and a JSPS Research Fellowship.

[1] a) A. Dragulescu-Andrasi, J. Rao, *ChemBioChem* **2007**, *8*, 1099–1101; b) H. M. O'Hare, K. Johnsson, A. Gautier, *Curr. Opin. Struct. Biol.* **2007**, *17*, 488–494.

[2] a) I. Chen, M. Howarth, W. Lin, A. Y. Ting, *Nat. Methods* **2005**, *2*, 99–104; b) C. W. Lin, A. Y. Ting, *J. Am. Chem. Soc.* **2006**, *128*, 4542–4543; c) J. Yin, F. Liu, X. Li, C. T. Walsh, *J. Am. Chem. Soc.* **2004**, *126*, 7754–7755; d) N. George, H. Pick, H. Vogel, N. Johnsson, K. Johnsson, *J. Am. Chem. Soc.* **2004**, *126*, 8896–8897; e) H. Mao, S. A. Hart, A. Schink, B. A. Pollok, *J. Am. Chem. Soc.* **2004**, *126*, 2670–2671; f) T. Tanaka, T. Yamamoto, S. Tsukiji, T. Nagamune, *ChemBioChem* **2008**, *9*, 802–807.

[3] a) B. A. Griffin, S. R. Adams, R. Y. Tsien, *Science* **1998**, *281*, 269–272; b) S. R. Adams, R. E. Campbell, L. A. Gross, B. R. Martin, G. K. Walkup, Y. Yao, J. Llopis, R. Y. Tsien, *J. Am. Chem. Soc.* **2002**, *124*, 6063–6076; c) H. Nonaka, S. Fujishima, S. Uchinomiya, A. Ojida, I. Hamachi, *J. Am. Chem. Soc.* **2010**, *132*, 9301–9309; d) E. G. Guignet, R. Hovius, H. Vogel, *Nat. Biotechnol.* **2004**, *22*,

440–444; e) T. L. Halo, J. Appelbaum, E. M. Hobert, D. M. Balkin, A. Schepartz, *J. Am. Chem. Soc.* **2009**, *131*, 438–439.
[4] a) A. Keppler, S. Gendreizig, H. Pick, H. Vogel, K. Johnsson, *Nat. Biotechnol.* **2003**, *21*, 86–89; b) A. Keppler, H. Pick, C. Arrivoli, H. Vogel, K. Johnsson, *Proc. Natl. Acad. Sci. USA* **2004**, *101*, 9955–9959; c) G. V. Los, L. P. Encell, M. G. McDougall, D. D. Hartzell, N. Karassina, C. Zimprich, M. G. Wood, R. Learish, R. F. Ohana, M. Urh, D. Simpson, J. Mendez, K. Zimmerman, P. Otto, G. Vidugiris, J. Zhu, A. Darzins, D. H. Klaubert, R. F. Bulleit, K. V. Wood, *ACS Chem. Biol.* **2008**, *3*, 373–382; d) L. W. Miller, J. Sable, P. Goelet, M. P. Sheetz, V. W. Cornish, *Angew. Chem.* **2004**, *116*, 1704–1707; *Angew. Chem. Int. Ed.* **2004**, *43*, 1672–1675; e) Y. Hori, H. Ueno, S. Mizukami, K. Kikuchi, *J. Am. Chem. Soc.* **2009**, *131*, 16610–16611.
[5] M. J. Hinner, K. Johnsson, *Curr. Opin. Biotechnol.* **2010**, *21*, 766–776.
[6] a) S. Mizukami, S. Watanabe, Y. Hori, K. Kikuchi, *J. Am. Chem. Soc.* **2009**, *131*, 5016–5017; b) S. Watanabe, S. Mizukami, Y. Hori, K. Kikuchi, *Bioconjugate Chem.* **2010**, *21*, 2320–2326; c) K. K. Sadhu, S. Mizukami, S. Watanabe, K. Kikuchi, *Chem. Commun.* **2010**, *46*, 7403–7405.
[7] H. Christensen, T. M. Martin, S. G. Waley, *Biochem. J.* **1990**, *266*, 853–861.
[8] M. Rooseboom, J. N. M. Commandeur, N. P. E. Vermeulen, *Phamacol. Rev.* **2004**, *56*, 53–102.
[9] L. Varetto, F. De Meester, D. Monnaie, J. Marchand-Brynaert, G. Dive, F. Jacob, J. M. Frere, *Biochem. J.* **1991**, *278*, 801–807.
[10] G. N. Rolinson, *J. Antimicrob. Chemother.* **1986**, *17*, 5–36.
[11] a) N. O. Bodin, B. Ekström, U. Forsgren, L. P. Jalar, L. Magni, C. H. Ramsay, B. Sjöberg, *Antimicrob. Agents Chemother.* **1975**, *8*, 518–525; b) J. Sjövall, L. Magni, T. Bergan, *Antimicrob. Agents Chemother.* **1978**, *13*, 90–96; c) J. Sjövall, L. Magni, E. Vinnars, *Antimicrob. Agents Chemother.* **1981**, *20*, 837–838; d) J. M. Ensink, A. G. Vulto, A. S. J. P. A. M. van Miert, J. J. Tukker, M. B. U. Winkel, M. A. H. M. Fluitman, *Am. J. Vet. Res.* **1996**, *57*, 1021–1024.
[12] A kind gift from Nichi-iko Phamaceutical Co., Ltd.
[13] A. Stańczak, A. Ferra, *Pharmacol. Rep.* **2006**, *58*, 599–613.
[14] H. Takakusa, K. Kikuchi, Y. Urano, H. Kojima, T. Nagano, *Chem. Eur. J.* **2003**, *9*, 1479–1485.
[15] R. P. Ambler, G. K. Scott, *Proc. Natl. Acad. Sci. USA* **1978**, *75*, 3732–3736.
[16] J. T. Moore, S. T. Davis, I. K. Dev, *Anal. Biochem.* **1997**, *247*, 203–211.
[17] M. Kozak, *J. Cell Biol.* **1991**, *115*, 887–903.
[18] D. Kalderon, B. L. Roberts, W. D. Richardson, A. E. Smith, *Cell* **1984**, *39*, 499–509.
[19] V. L. Johnson, L. M. Walsh, B. L. Chen, *Proc. Natl. Acad. Sci. USA* **1980**, *77*, 990–994.
[20] S. Svendsen, C. Zimprich, M. G. McDougall, D. H. Klaubert, G. V. Los, *Promega Notes* **2007**, *95*, 16–19.
[21] A. P. Laws, N. J. Layland, D. G. Proctor, M. I. Page, *J. Chem. Soc. Perkin Trans. 2* **1989**, *10*, 1577–1581.
[22] Y. Nishikawa, K. Hiraki, *Analytical Methods of Fluorescence and Phosphorescence*, Kyoritsu Publishing Company, Tokyo, **1984**.
[23] C. A. Parker, W. T. Rees, *Analyst* **1960**, *85*, 587–600.

Received: March 30, 2011
Published online: June 8, 2011

Cell Imaging Technology

DOI: 10.1002/anie.201103775

Covalent Protein Labeling with a Lanthanide Complex and Its Application to Photoluminescence Lifetime-Based Multicolor Bioimaging**

*Shin Mizukami, Taku Yamamoto, Akimasa Yoshimura, Shuji Watanabe, and Kazuya Kikuchi**

Long-lifetime photoluminescence (PL) enables the use of time-resolved (TR) measurements, which can eliminate short-lifetime luminescent signals.[1] Thus, lanthanide luminescence measurement has been utilized as a highly sensitive biochemical assay technique.[2] Recent progress in optical instrumentation has enabled the development of time-resolved luminescence (TRL) microscopy with pulse excitation techniques,[3] making lanthanide-based TRL imaging of biomolecules a promising technology for next-generation bioimaging. Recently, a TRL-based protein imaging technique was reported.[4] This system exploits a protein labeling system based on *Escherichia coli* dihydrofolate reductase and its specific inhibitors modified with a lanthanide complex. Because this system uses a noncovalent enzyme-inhibitor complex model,[5] dissociation of the labeled probe from the tag protein is a potential limitation, especially for long time-lapse imaging over several hours.

We recently developed a versatile protein labeling method using a mutant TEM-1 β-lactamase (BL-tag) and its fluorescent substrates.[6] By extending this covalent labeling technology, we aimed to develop a TRL imaging method for cell-surface proteins (Figure 1a). We designed and synthesized a novel luminescent europium(III) complex probe, TPA-Eu (Figure 1b and Scheme S1 in the Supporting Information). This compound consists of a terpyridinetetraacetate Eu^{3+} complex[7] connected to an ampicillin moiety, which covalently binds BL-tag.[6a] The wavelengths of excitation and emission maxima of TPA-Eu were 341.5 and 616.0 nm, respectively (Figure 1c). The emission spectrum was characteristic of Eu^{3+} luminescence. The luminescence lifetime was 1.25 ms (Figure S2 in the Supporting Information), which is long enough for TRL microscopy with a xenon flash lamp.

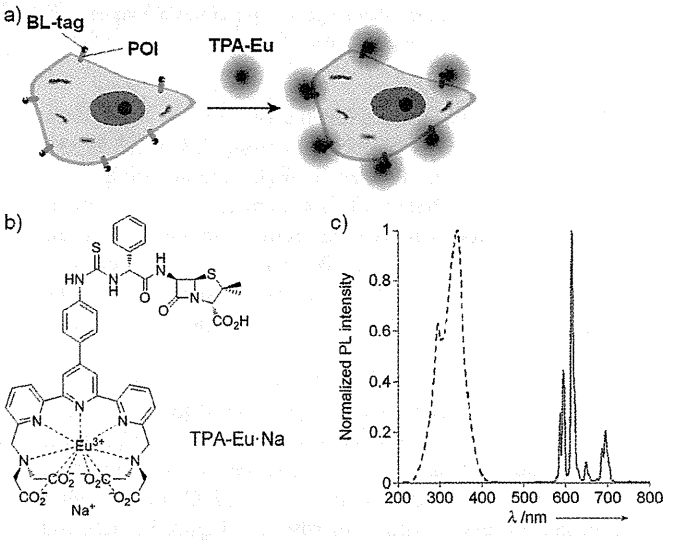

Figure 1. a) Covalent labeling of cell-surface protein of interest (POI) with a luminescent lanthanide complex for time-resolved photoluminescence imaging. b) Structure of TPA-Eu. c) Normalized steady-state excitation (---, λ_{em} = 616.0 nm), steady-state emission (——, λ_{ex} = 341.5 nm), and TR emission (-----, λ_{ex} = 341.5 nm, delay time: 60 μs, gate time: 2 ms) spectra of 10 μM TPA-Eu in 100 mM HEPES buffer (pH 7.4) at 25 °C; HEPES: 2-[4-(2-hydroxyethyl)-1-piperazinyl]ethanesulfonic acid.

Next, the tag-labeling properties of TPA-Eu were investigated. TPA-Eu was incubated with BL-tag or wild-type TEM-1 (WT TEM) for 1 h, and the mixtures were analyzed by SDS-PAGE. Red PL of TPA-Eu labeled with the BL-tag was observed, but no labeling with WT TEM was seen (Figure 2a,b). The cell lysate did not interfere with labeling specificity (Figure 2c). Covalent labeling was also confirmed by MALDI-TOF MS. The mass spectrum of TPA-Eu-labeled BL-tag showed that TPA-Eu bound to the tag with a 1:1 stoichiometry (Table S1 in the Supporting Information). The PL spectra and lifetime of TPA-Eu labeled with BL-tag were measured, and both excitation and emission spectra were found to be almost identical to those of free TPA-Eu (data not shown), while the PL lifetime of the labeled TPA-Eu was also scarcely changed (1.27 ms, Figure S2 in the Supporting Information). These results indicated that TPA-Eu labeled with the tag protein maintained the photophysical properties of free TPA-Eu.

[*] Dr. S. Mizukami, T. Yamamoto, A. Yoshimura, S. Watanabe, Prof. K. Kikuchi
Graduate School of Engineering
Osaka University, Osaka 565-0871 (Japan)
E-mail: kkikuchi@mls.eng.osaka-u.ac.jp
Homepage: http://www-molpro.mls.eng.osaka-u.ac.jp/
Dr. S. Mizukami, Prof. K. Kikuchi
Immunology Frontier Research Center (IFReC)
Osaka University, Osaka 565-0871 (Japan)

[**] We thank Shigeru Kobayashi at Olympus Engineering Co. Ltd. for his technical help in constructing the TRL microscopy system. This work was supported by MEXT of Japan, by the Funding Program for World-Leading Innovative R&D on Science and Technology from JSPS, by CREST from JST, and by Asahi Glass Foundation.

Supporting information for this article is available on the WWW under http://dx.doi.org/10.1002/anie.201103775.

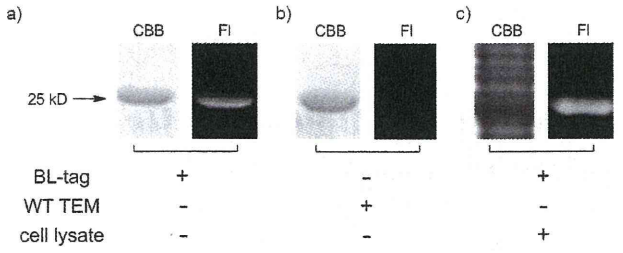

Figure 2. Specific labeling of BL-tag with TPA-Eu. a) BL-tag, b) WT TEM, and c) BL-tag mixed with HEK293T cell lysate were analyzed by electrophoresis. Fluorescent gel images were excited with a handheld UV lamp (λ_{ex} = 365 nm). CBB-stained gel image; CBB: Coomassie Brilliant Blue; Fl: fluorescent gel image.

TRL microscopy measurements of TPA-Eu were then performed. The TRL microscopy system (Figure S3 in the Supporting Information) was a slight modification of a reported system.[3b] Because this system excludes any short-lifetime luminescent signals, long-lifetime luminescent signals can be selectively detected. We confirmed the selective detection of long-lifetime PL of TPA-Eu over short-lifetime PL using silica gels (Figure S4d in the Supporting Information).

We next analyzed TPA-Eu-labeled cellular proteins using the TR microscopy system. BL-tag was fused to the extracellular region (N terminus) of epidermal growth factor receptor (EGFR) and expressed in HEK293T cells. The cells were treated with 10 μM TPA-Eu for 1 h at 37 °C, washed with buffer, and observed with a microscope (Figure 3a, left and center columns). Under UV excitation (λ = 340–390 nm), cellular autofluorescence severely interfered with the short-lifetime PL signals from TPA-Eu in the total PL images, which include no delay time, thereby providing almost identical results to steady-state measurements. On the other hand, the delayed PL images detected only TPA-Eu-labeled BL-EGFR. No long-lifetime PL was observed from the cells not expressing BL-EGFR.

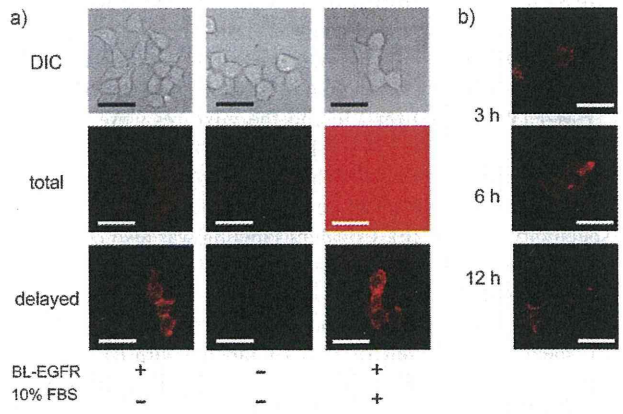

Figure 3. a) Microscopy images of HEK293T cells labeled with TPA-Eu. DIC: differential interference contrast images, total: total PL images, delayed: delayed PL images. b) Time-lapse imaging of HEK293T cells expressing BL-EGFR labeled with TPA-Eu. Incubation times are shown beside TR microscopy images. Scale bar: 50 μm.

The cells were also observed in the presence of 10% fetal bovine serum (FBS, Figure 3a, right column). In the total PL image, various fluorescent components in FBS interfered with the visualization of the TPA-Eu-labeled target proteins. However, the delayed PL image showed only long-lifetime components of the TPA-Eu signals on the cell surface. This property is useful for general bioimaging studies, because the inclusion of serum would enhance the robustness of living samples and would enable imaging over long periods. Long time-lapse imaging experiments, which can be performed in the presence of FBS, demonstrated no distinct dissociation of the labeled TPA-Eu from the target protein even after several hours (Figure 3b). This result demonstrated one of the advantages of our covalent-labeling-based method over previous technologies.[4]

Finally, we tested the application of TPA-Eu to lifetime-based multicolor imaging. As illustrated in Figure 4a, short- and long-lifetime PL signals, generated by organic dyes and lanthanide complexes, respectively, can be discriminately detected by the time-resolved gating technique, even if their emission spectra mostly overlap. After verifying the principle by using silica gels (Figure S3c–e in the Supporting Information), HEK293T cells expressing BL-EGFR were simultaneously labeled with TPA-Eu and MitoTracker Orange (MTO), which is a rhodamine-based fluorescent dye that stains mitochondria. The short-lifetime fluorescence of MTO was selectively visualized by accumulating the prompt PL component (delay time: 0 s, gate time: 10 μs; Figure 4c), while the long-lifetime PL of TPA-Eu on the cell-surface BL-EGFR was selectively detected as a delayed PL component

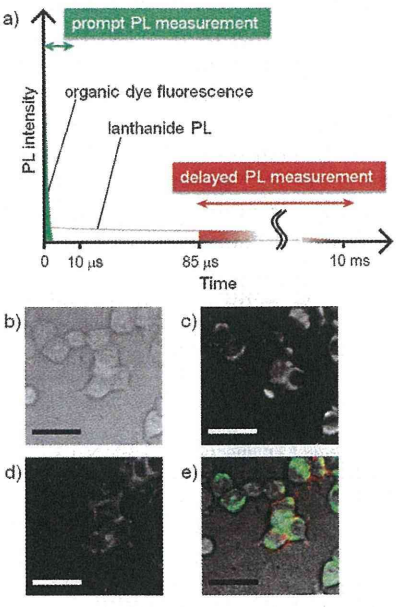

Figure 4. a) Illustration of time-gating discrimination of short- (organic fluorophores) and long-lifetime (lanthanides) luminescence components. b)–e) Lifetime-based multicolor imaging. Scale bar: 50 μm. b) DIC, c) prompt PL image, d) delayed PL image, and e) merged image. Short (MTO) and long (TPA-Eu) lifetime PL components were drawn with different pseudocolors (pseudo color: green for prompt PL and red for delayed PL).

(delay time: 85 μs, gate time: 10 ms; Figure 4d). These two signals can be overlaid with different pseudocolors (Figure 4e). Although frequency-domain fluorescence lifetime imaging microscopy (FLIM)[8] is an existing similar technique utilizing fluorescence lifetimes, this method requires a much longer accumulation time than our technique and also has the disadvantage of its high cost.

In conclusion, we have developed a novel protein imaging system based on covalent protein labeling with the lanthanide probe TPA-Eu combined with TRL microscopy. This technology separates live-cell imaging from background autofluorescence. The long-lifetime PL of TPA-Eu labels on cell-surface proteins can be selectively detected even in the presence of FBS. The covalent probe labeling enabled long time-lapse imaging lasting at least several hours. Both of these virtues are quite valuable especially for in vivo imaging experiments, because the autofluorescence of animal bodies severely hampers detection of faint PL signals, and in vivo studies usually take at least several hours. For further applications, intracellular protein labeling may be desired. As we expected from the anionic structure, TPA-Eu did not permeate into living cells. More hydrophobic or cationic lanthanide complexes should be chosen for intracellular protein labeling.

We also demonstrated a unique application—lifetime-based multicolor imaging—by exploiting pulse-gating technology. This multicolor imaging system would yield almost the same data as multicolor fluorescence imaging with different filter sets. Because this technique is orthogonal to the conventional wavelength-based multicolor imaging, simultaneous use of both wavelength-based and lifetime-based multicolor imaging techniques could increase the number of color channels. For example, three emission filter sets (blue, green, and red) and two lifetime settings (short and long) yield six channels. Considering that differently colored luminescent lanthanides such as terbium(III) or dysprosium(III) are also suitable for TRL measurements, simultaneous imaging of a larger number of proteins can be achieved in future.

Received: June 3, 2011
Published online: July 26, 2011

Keywords: imaging agents · labeling probes · proteins · time-resolved luminescence

[1] a) J. C. G. Bünzli, C. Piguet, *Chem. Soc. Rev.* **2005**, *34*, 1048–1077; b) J. Yuan, G. Wang, *Trends Analyt. Chem.* **2006**, *25*, 490–500.

[2] a) J. C. G. Bünzli, *Chem. Rev.* **2010**, *110*, 2729–2755; b) R. A. Kumar, D. S. Clark, *Curr. Opin. Chem. Biol.* **2006**, *10*, 162–168; c) J. Karvinen, V. Laitala, M. L. Mäkinen, O. Mulari, J. Tamminen, J. Hermonen, P. Hurskainen, I. Hammilä, *Anal. Chem.* **2004**, *76*, 1429–1436; d) T. Terai, K. Kikuchi, S. Iwasawa, T. Kawabe, Y. Hirata, Y. Urano, T. Nagano, *J. Am. Chem. Soc.* **2006**, *128*, 6938–6946; e) S. Mizukami, K. Tonai, M. Kaneko, K. Kikuchi, *J. Am. Chem. Soc.* **2008**, *130*, 14376–14377; f) D. Maurel, L. C. Agrar, C. Brock, M. L. Rives, E. Bourrier, M. A. Ayoub, H. Bzin, N. Tinel, T. Drroux, L. Prézeau, E. Trinquet, J. P. Pin, *Nat. Methods* **2008**, *5*, 561–567; g) L. Albizu, M. Cottet, M. Kralikova, S. Stoev, R. Seyer, I. Brabet, T. Roux, H. Bazin, E. Bourrier, L. Lamarque, C. Breton, M. L. Rives, A. Newman, J. Javitch, E. Trinquet, M. Manning, J. P. Pin, B. Mouillac, T. Durroux, *Nat. Chem. Biol.* **2010**, *6*, 587–594.

[3] a) N. Gahlaut, L. W. Miller, *Cytometry Part A* **2010**, *77A*, 1113–1125; b) K. Hanaoka, K. Kikuchi, S. Kobayashi, T. Nagano, *J. Am. Chem. Soc.* **2007**, *129*, 13502–13509.

[4] a) H. E. Rajapakse, D. R. Reddy, S. Mohandessi, N. G. Butlin, L. W. Miller, *Angew. Chem.* **2009**, *121*, 5090–5092; *Angew. Chem. Int. Ed.* **2009**, *48*, 4990–4992; b) H. E. Rajapakse, N. Gahlaut, S. Mohandessi, D. Yu, J. R. Turner, L. W. Miller, *Proc. Natl. Acad. Sci. USA* **2010**, *107*, 13582–13587.

[5] a) L. W. Miller, Y. Cai, M. P. Sheetz, V. W. Cornish, *Nat. Methods* **2005**, *2*, 255–257; b) N. T. Calloway, M. Choob, A. Sanz, M. P. Sheetz, L. W. Miller, V. W. Cornish, *ChemBioChem* **2007**, *8*, 767–774.

[6] a) S. Mizukami, S. Watanabe, Y. Hori, K. Kikuchi, *J. Am. Chem. Soc.* **2009**, *131*, 5016–5017; b) S. Watanabe, S. Mizukami, Y. Hori, K. Kikuchi, *Bioconjugate Chem.* **2010**, *21*, 2320–2326; c) K. K. Sadhu, S. Mizukami, S. Watanabe, K. Kikuchi, *Chem. Commun.* **2010**, *46*, 7403–7405.

[7] a) V. M. Mukkala, M. Helenius, I. Hemmilä, J. Kankare, H. Takalo, *Helv. Chim. Acta* **1993**, *76*, 1361–1378; b) T. Nishioka, J. Yuan, Y. Yamamoto, K. Sumitomo, Z. Wang, K. Hashino, C. Hosoya, K. Ikawa, G. Wang, K. Matsumoto, *Inorg. Chem.* **2006**, *45*, 4088–4096; c) B. Song, G. Wang, M. Tan, J. Yuan, *J. Am. Chem. Soc.* **2006**, *128*, 13442–13450.

[8] a) E. B. Munster, T. W. J. Gadella, *Adv. Biochem. Eng./Biotechnol.* **2005**, *95*, 143–175; b) Y. C. Chen, R. M. Clegg, *Photosynth. Res.* **2009**, *102*, 143–155; c) J. W. Borst, A. J. W. G. Visser, *Meas. Sci. Technol.* **2010**, *21*, 102002–102022; d) D. W. Piston, G. J. Kremers, *Trends Biochem. Sci.* **2007**, *32*, 407–414; e) J. Goedhart, L. V. Weeren, M. A. Hink, N. O. E. Vischer, K. Jalink, T. W. J. Gadella Jr. , *Nat. Methods* **2010**, *7*, 137–139; f) R. Pepperkok, A. Squire, S. Geley, P. I. H. Bastiaens, *Curr. Biol.* **1999**, *9*, 269–274.

Molecular BioSystems

View Online
Dynamic Article Links

Cite this: *Mol. BioSyst.*, 2011, **7**, 1766–1772

www.rsc.org/molecularbiosystems

PAPER

Sequential ordering among multicolor fluorophores for protein labeling facility *via* aggregation-elimination based β-lactam probes†

Kalyan K. Sadhu,[a] Shin Mizukami,[ab] Shuji Watanabe[a] and Kazuya Kikuchi*[ab]

Received 12th January 2011, Accepted 24th February 2011
DOI: 10.1039/c1mb05013c

Development of protein labeling techniques with small molecules is enthralling because this method brings promises for triumph over the limitations of fluorescent proteins in live cell imaging. This technology deals with the functionalization of proteins with small molecules and is anticipated to facilitate the expansion of various protein assay methods. A new straightforward aggregation and elimination-based technique for a protein labeling system has been developed with a versatile emissive range of fluorophores. These fluorophores have been applied to show their efficiency for protein labeling by exploiting the same basic principle. A genetically modified version of class A type β-lactamase has been used as the tag protein (BL-tag). The strength of the aggregation interaction between a fluorophore and a quencher plays a governing role in the elimination step of the quencher from the probes, which ultimately controls the swiftness of the protein labeling strategy. Modulation in the elimination process can be accomplished by the variation in the nature of the fluorophore. This diversity facilitates the study of the competitive binding order among the synthesized probes toward the BL-tag labeling method. An aggregation and elimination-based BL-tag technique has been explored to develop an order of color labeling from the equimolar mixture of the labeling probe in solutions. The qualitative and quantitative determination of ordering within the probes toward labeling studies has been executed through SDS-PAGE and time-dependent fluorescence intensity enhancement measurements, respectively. The desirable multiple-wavelength fluorescence labeling probes for the BL-tag technology have been developed and demonstrate broad applicability of this labeling technology to live cell imaging with coumarin and fluorescein derivatives by using confocal microscopy.

Introduction

In recent years, research with photosensitive molecular probes possessing high selectivity has been used for analyzing cellular processes with several potential applications.[1] The use of genetically encoded fluorescent tags has drawn attention toward the subcellular distributions of many proteins.[2] An advanced technique to bring forth photosensitive proteins is the site-specific labeling of proteins with tailor-made photosensitive small probes. Several protein mediated labeling methods such as the tetracysteine tag,[3] the HaloTag,[4] the SNAP-tag,[5] tetraaspartate,[6] α-bungarotoxin binding peptide,[7] combination of tetraserine and bisboronic acid,[8] and dihydrofolate reductase[9] are known in literature. The method based on single-chain variable fragment (scFv) antibodies and non-covalently bound fluorogenic dyes was developed.[10] Proficiency in molecular biology furnishes the development of probe designing, and this blending can enable the modification of labeling experiments. The coalescence of two orthogonal tagging methods provides access to develop new labeling experiments due to their simultaneous performance. We have recently shown simultaneous orthogonal labeling of our technique and the SNAP-tag in cell imaging studies.[11] Other reports depict the generation of fluorescent labeling techniques that can be exclusively conjugated to SNAP-tag fusion proteins.[1h,12] The choice of color for studying the dynamic processes in different domains of mammalian cells would be improvised with multifaceted fluorophores for each of the merged labeling techniques. Our current approach will be helpful to modify the technique for multicolor labeling with a genetically modified β-lactamase protein. In this present work, we have developed a new technique to determine an order of the studied probes in the labeling efficiency, which ensued from the aggregation interaction energies between the fluorophore and the quencher.

In our earlier studies we have depicted a novel protein labeling system by conglutination of genetically modified β-lactamase

[a] *Division of Advanced Science and Biotechnology, Graduate School of Engineering, Osaka University, 2-1 Yamadaoka, Suita, Osaka 565-0871, Japan. E-mail: kkikuchi@mls.eng.osaka-u.ac.jp; Web: http://www-molpro.mls.eng.osaka-u.ac.jp/; Fax: (+81) 6-6879-7875*
[b] *Immunology Frontier Research Center, Osaka University, 3-1 Yamadaoka, Suita, Osaka 565-0871, Japan*

† Electronic supplementary information (ESI) available: Experimental details, chemical structures, UV-Visible absorption spectra, and fluorescence spectra of the probes. See DOI: 10.1039/c1mb05013c.

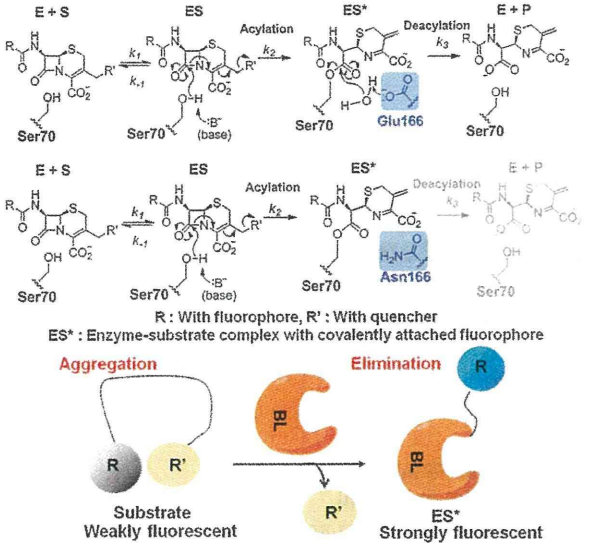

Scheme 1 Reaction mechanism of WT TEM (top) and BL-tag technique (middle) *via* control of deacylation step for protein labeling by E166N point mutation of class A β-lactamase; (E) enzyme, (S) substrate, and (P) product; general mechanism of protein labeling through covalent bond using BL-tag (bottom).

(BL-tag, Scheme 1) with low-molecular-weight fluorogenic β-lactam probes.[1e,11,13] In BL-tag technology, the acyl-enzyme intermediate (Scheme 1) is accumulated by markedly slowing the deacylation step[14] relative to the acylation step with wild-type (WT) TEM-1 (class A type β-lactamase, hereafter, WT TEM). We have successfully exploited this property of the mutant to covalently attach a fluorescent substrate with genetically modified β-lactamase for the protein labeling technique. We have also shown that the aggregation and elimination-based strategy is selectively applicable to the BL-tag labeling method.[13] Highly specific covalent labeling properties of this technology are anticipated to furnish robust tools for investigating protein functions. These probes have been ascertained to be more beneficial for fluorogenicity and specificity compared to the available green fluorescent proteins. Low invasiveness with respect to the functions of the epidermal growth factor receptor (EGFR) has been corroborated by this technique. With suitable sensitivity and swiftness of labeling, this strategy might be applicable to study protein trafficking *in vivo*.

To outstrip the limitations of our FRET-based process,[1e,11] we have recently developed a new approach based on the switching mechanism involving aggregation followed by elimination processes between a fluorophore and a quencher[13] (Scheme 1). Now, we have used this straightforward technique for the generation of controllable color variation in fluorogenic probes, with a wide range of emission wavelengths, suitable for protein labeling in living cells. The advantage of this design principle is robustness toward any fluorophore whose fluorescence intensity was not easily modified by the previous FRET-based design. In this development stage of the tailored version, we have developed a multiple color palette with different fluorophores such as coumarin, and 5- and 6-carboxyrhodamine derivatives, which support the fact that the system does not necessitate any restriction in fluorophore choice anymore as the system adopts the aggregation quenching principle. We have continued our strategy with the *m*-dinitrobenzene (DNB) group as the quencher to study the effect of aggregation interactions toward the fluorescence enhancement of the probes with a wide range of emissive fluorophores, which ultimately controls the quencher elimination step from the probe. The structures of the newly synthesized probes vary only in the fluorophoric part in our recent strategic compounds. The developed order in the BL-tag labeling efficiency of the probes is the final outcome of the moderated disaggregation steps of the probe reaction.

Results and discussion

Design and synthesis

The practical utility of the fluorescently labeled BL-tag under a physiological situation has been explored with the newly synthesized three cephalosporin-based fluorescent probes with coumarin (**CCDNB**, Scheme 2) and rhodamine isomers (**5RCDNB** and **6RCDNB**, Scheme 2). We have compared the fluorogenic nature of our new probes with a previous[13] fluorescein analog (**FCDNB**, Scheme 2).

The polyethylene glycol (PEG) spacer was used to ascertain the aggregation between the fluorophore and the quencher in each case. The PEG spacer is also beneficial for attaining a flexible structure of the probes for favorable aggregation interactions among fluorophores and quenchers. The syntheses of **CCDNB**, **5RCDNB**, and **6RCDNB** were performed using similar procedures to our earlier studies with **FCDNB**.[13] The succinimidyl ester of coumarin and 5(6)-carboxytetramethyl

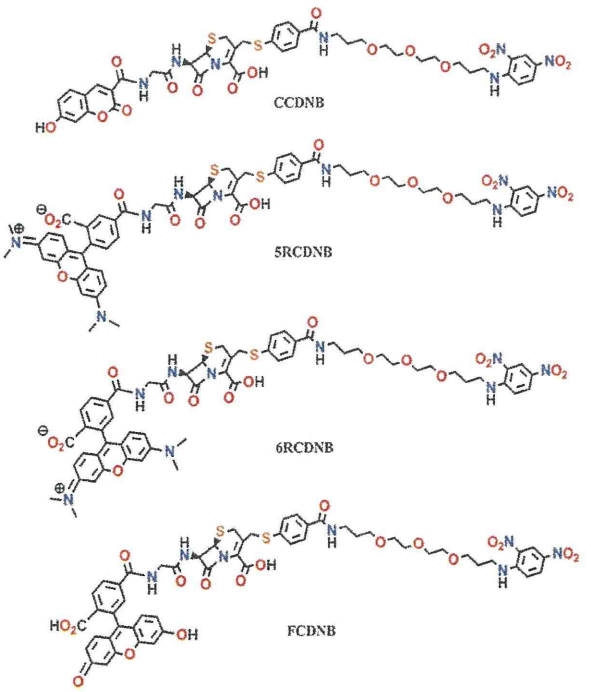

Scheme 2 Chemical structures of synthesized fluorescent probes with different colored tags for protein labeling.

rhodamine were used for corresponding probe syntheses. Final rhodamine isomeric products were separated from their mixture by preparative HPLC. The purities of all the final compounds were checked by analytical HPLC (Fig. S4–S6, ESI†), ^{1}H NMR, ^{13}C NMR, and HR-FAB-MS.

Absorption and emission studies of the free probes

Absorption studies of **CCDNB**, **5RCDNB**, and **6RCDNB** (Fig. 1) were checked in the 100 mM HEPES buffer (pH 7.4) and in methanol. The interaction between the fluorophores and the quencher is reflected in the absorption maxima of the probes in these two solvents. The maximum interaction was observed in the case of the **CCDNB** probe in the HEPES buffer. Under this physiological condition the absorption peaks of coumarin and the DNB group in **CCDNB** were obtained at 407 and 375 nm respectively. In methanol, the absorption peaks for coumarin remained at the same position, whereas the peak position of DNB was blue shifted and observed at 351 nm (Fig. S7a, ESI†). The literature reported that the absorption peak due to free *N*-ethyl-substituted 2,4-dinitroaniline[15] in methanol was quite similar to our observed value in methanol. The large shift of the DNB group with a low extinction coefficient value in an aqueous medium compared to the value reported in the literature[16] was due to the favorable aggregation interaction between coumarin and the DNB quencher in a physiological pH medium. In the case of both the rhodamine isomers, the absorption peaks of rhodamine and the DNB group were obtained at 559 and 359 nm, respectively, in the HEPES buffer. In methanol, the absorption peaks for both the DNB group and rhodamine were blue shifted by 5–15 nm (Fig. S7b, ESI†). This observation was similar to our previous finding with fluorescein derivatives in **FCDNB**.[13] The well-known capacity of the DNB group to form π-stack complexes raises the possibility that aggregation interaction of this type might contribute to the unusual stability of some fluorophore–quencher complexes.

The emission spectra of the free probes were measured in physiological pH buffer (Fig. 1) and compared with those in methanol. The fluorescence quantum yields of all the probes were significantly quenched in the 100 mM HEPES buffer (Table 1). In the aggregated form, the amount of interaction energy between the fluorogenic parts of different probes and the quencher restricts the emission of the fluorophore, which is reflected in the low quantum yield of the probes under physiological conditions. 2,4-Dinitroaniline is an efficient intramolecular fluorescence quencher for fluorophores with different emissive regions.[17] The mechanism of emission restriction might be thought to arise from the π-stacking interaction between highly electron-rich fluorophores and electron-deficient nitroaromatics. The reported electron density calculations attributing to the quenching phenomenon of the DNB group suggests electron deficiency on the DNB part.[18] Theoretical calculations involving interaction energies between the indirectly correlated groups with the DNB group confirm its legitimacy to the rational association between the substituted groups and the molecular stabilities.[19] The inherent quenching phenomenon of DNB, which does not depend upon the nature of fluorophores but rather upon the aggregation technique, has been found to be effective for several fluorogenic probes. The quantum yields of the same probes were much higher in methanol (Table 1). This significant difference in emissions in these two solutions (Fig. S8a and S8b, ESI†) implies that the aggregation phenomenon is favorable only in the aqueous buffer solution (Fig. S8c, ESI†).

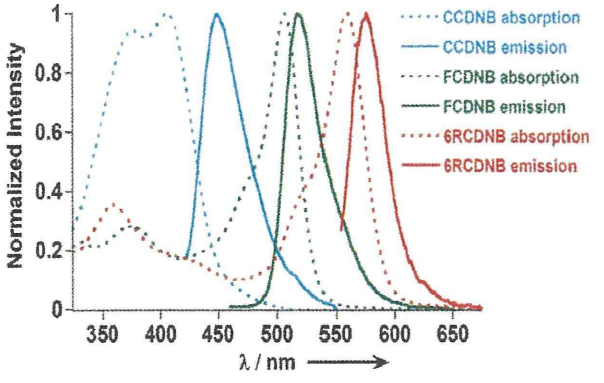

Fig. 1 Multicolor absorption and emission region involved in the aggregation-elimination strategy for BL-tag; normalized absorption and emission spectra of each probes in 100 mM HEPES buffer (pH 7.4).

Emission studies of the probes in the presence of the tag protein

To observe the fluorogenicity of the synthesized probes, the emission spectra of each probe were studied in the presence of the BL-tag and WT TEM. The reaction in the presence of WT TEM is catalytic in nature, whereas the BL-tag reaction is non-catalytic. In the presence of the BL-tag, the quencher part was eliminated from the **CCDNB** probe according to our recently developed strategy.[13] This elimination process was reflected in the fluorescence enhancement of the coumarin probe in the course of the reaction between the probe and the BL-tag with time (Fig. 2a). The fluorescence intensity at 450 nm due to coumarin (λ_{ex} = 407 nm) was monitored (Fig. 2b) after the incubation of BL-tag with **CCDNB**. In the case of both the rhodamine isomers, the monitored emission wavelength was 575 nm (λ_{ex} = 558 nm) (Fig. 2c and d). Significantly different enhancement rates of fluorescence intensities were observed with time for different fluorophoric parts in successive probes (Fig. 3b–d). The elimination step for each probe was similar in nature as the DNB quencher was used in all cases. The difference in the fluorescence enhancement rate indicates that the amount of aggregation energy between the fluorophores and the quencher is different in each case due to the accessibility of different fluorophores in the probes to the enzyme active site and this interaction curtails the next step involving disaggregation followed by elimination of the DNB group. The aggregation interaction is governed by the electron density as well as the steric bulk of the fluorophore and the quencher part, which is expected to vary with the nature of the fluorophore, as the quencher remains the same for all studied probes. Substantial increase in the fluorescence enhancement rate is observed in the case of the incubation study with WT TEM compared

Table 1 Fluorescence quantum yields of the synthesized probes in physiological pH buffer and in methanol

Solvent	Fluorescence quantum yield			
	CCDNB	**5RCDNB**	**6RCDNB**	**FCDNB**[13]
100 mM HEPES buffer (pH 7.4)	0.04	0.04	0.06	0.05
Methanol	0.19	0.24	0.25	0.42

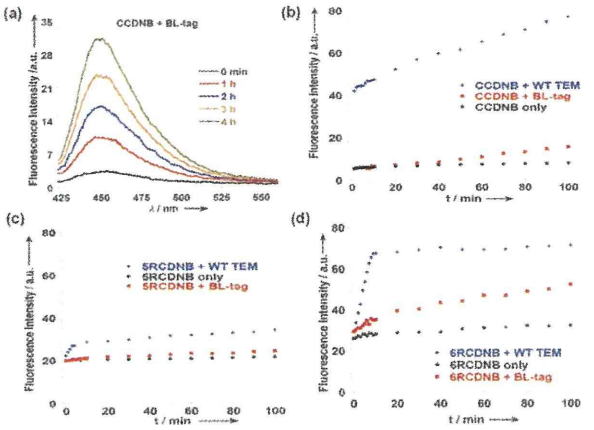

Fig. 2 (a) Time-dependent emission spectra (λ_{ex} = 407 nm) of **CCDNB** (conc. of **CCDNB**: 1.0 μM) in the presence of BL-tag in 100 mM HEPES buffer (pH 7.4) containing 0.1% DMSO at 25 °C. (b–d) Change in fluorescence intensities of (b) **CCDNB** (conc. of **CCDNB**: 1.0 μM, and λ_{ex} = 407 nm), (c) **5RCDNB** (conc. of **5RCDNB** 0.5 μM and λ_{ex} = 558 nm) and (d) **6RCDNB** (conc. of **6RCDNB**: 0.5 μM, and λ_{ex} = 558 nm) with time.

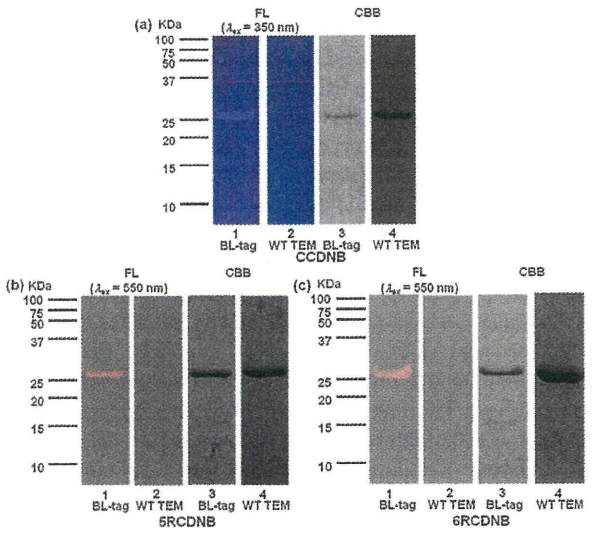

Fig. 3 Fluorescence (1 and 2) and CBB-stained (3 and 4) gel images of BL-tag and WT TEM β-lactamase incubated with (a) **CCDNB**, (b) **5RCDNB**, and (c) **6RCDNB**.

to BL-tag (Fig. 2) for all the probes as the reaction with WT TEM is catalytic in nature. The DNB group was eliminated by WT TEM at a faster rate, and the fluorescence signal increased as expected due to the favorable deacylation step in the catalytic mechanism. However, the enhancements in the fluorescence intensities in the case of different probes are not the same even in the presence of WT TEM. In the case of incubation of WT TEM with the probe **CCDNB**, 36% of the reaction was completed within 1 min, whereas in other cases this process was not so fast. Controlled elimination processes were observed when different probes with varying fluorophores were used, and the aggregation interaction between the fluorophore and the quencher is the guiding factor for such regulation. The initial rates of fluorescence enhancement in the case of WT TEM for all the probes were found to be much higher compared to the initial rates for the BL-tag. This noticeable difference in the reaction rates is mainly due to the combination of the controlled acylation path[20] and the ineffective catalytic deacylation step as a result of mutation at Glu166 of WT TEM.

Protein labeling *in vitro*

Incubation with the BL-tag protein leads to the subsequent elimination of the quencher in each probe and covalent modification of the tag protein with the desired color fluorophore. To check the versatile range of color monitoring *via* this method, SDS-PAGE studies were performed with coumarin- and rhodamine-based fluorogenic probes. The labeled protein was detected in each case by irradiating the gel with UV light (λ = 350 nm) for **CCDNB** and with visible light (λ = 550 nm) for **5RCDNB** and **6RCDNB** (Fig. 3). The corresponding labeled protein band of ~29 kDa was observed in each case. In these cases, similar experiments with WT TEM resulted in no labeled fluorescence in any case due to the lack of covalent linkage between the enzyme and the probe after the favorable deacylation step.

Qualitative ordering of labeling efficiencies of the probes

The only difference among the structures of probes is the nature of fluorophores. To check the possibility of different kinetic rates of protein labeling among the probes, several experiments were carried out. The control of the elimination step for different probes depends upon the aggregation interactions, which led to further studies to observe the effect of fluorophore in protein labeling by this new strategy. SDS-PAGE studies were carried out in several batches with the binary mixture of probes in an equimolar amount to show any preferential order of fluorophore labeling toward the BL-tag technique *via* the aggregation-elimination technique. The competitive labeling kinetics cannot distinguish between the two different kinetics steps involved: covalent interaction with the BL-tag and subsequent elimination of the quencher from the molecular probe; rather, it is a combined effect for overall labeling. To avoid confusion arising from the similar emissive region for rhodamine isomers, they were treated separately in the mixtures with the other probes. This qualitative study of

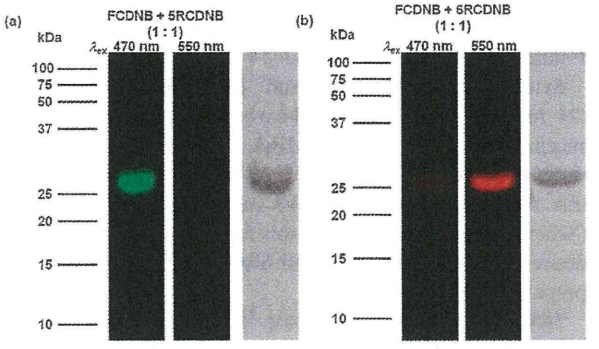

Fig. 4 Fluorescence (left) and CBB-stained (right) gel images of BL-tag incubated with (a) equimolar mixture of **5RCDNB** and **FCDNB** and (b) equimolar mixture of **6RCDNB** and **FCDNB**.

competitive protein labeling generates a preferential order among the fluorophores. From the mixture of the 5-rhodamine isomer and fluorescein derivatives, it was found that labeling was due to the fluorescein fluorophore (Fig. 4a). On the other hand, labeling was observed by the rhodamine fluorophore from the mixture of the 6-rhodamine isomer and fluorescein derivatives (Fig. 4b). These results conclude that the order of labeling probe is **6RCDNB** > **FCDNB** > **5RCDNB**. When the coumarin derivative was used in any binary mixture, the labeled protein showed the emission of coumarin irrespective of labeling by the other probes, except in the case of the 5-rhodamine isomer (Fig. S9 and S10, ESI†). In the case of a mixture of the coumarin derivative and the 5-rhodamine isomer, only coumarin fluorescence was observed without any rhodamine labeling. However, in the other cases, rhodamine and fluorescein fluorescence were observed from **6RCDNB** and **FCDNB**, respectively, along with the coumarin fluorescence when they were treated together with 1 : 1 molar ratio with **CCDNB**. The position of the coumarin derivative in the ordering of the probes could not be fixed from these qualitative SDS-PAGE studies. This result only supported the following labeling order: as **CCDNB** > **5RCDNB**. In the presence of an equimolar ternary mixture of **CCDNB**, **5RCDNB**, and **FCDNB**, the labeling due to coumarin and fluorescein was observed, without any fluorescence from rhodamine isomers. On the other hand, coumarin and rhodamine labeling were observed when a mixture of **CCDNB**, **6RCDNB**, and **FCDNB** was used (Fig. S11, ESI†).

Quantitative ordering of labeling efficiencies of the probes

All the qualitative results were further supported by the time-dependent fluorescence intensity measurement of the mixtures in the presence of the BL-tag. This quantitative measurement provided the order of labeling between all the probes from their mixtures. The fluorescence enhancement was monitored only at 450 nm (λ_{ex} = 407 nm) due to coumarin from its mixture with the other probes in the presence of the BL-tag (Fig. S12, ESI†). The enhancement rate supported the order of labeling obtained from SDS-PAGE studies for the rest of the probes. To find out the exact order of labeling efficiencies among **CCDNB**, **6RCDNB**, and **FCDNB**, fluorescence enhancement at 520 nm (λ_{ex} = 497 nm) and 575 nm (λ_{ex} = 558 nm) was monitored for the emission of fluorescein and 6-rhodamine, respectively, from the mixture of the probes. The fluorescence enhancement at 520 nm (Fig. 5a) suggests that the binding efficiency of **6RCDNB** is more compared to that of **CCDNB**. This is attributed to the lower fluorescence enhancement of fluorescein in the presence of the 6-rhodamine isomer compared to the case of fluorescein in the presence of the coumarin probe. A similar type of experiments used for the monitoring the fluorescent enhancement due to 6-rhodamine (Fig. 5b) was used to determine the binding efficiency order of the coumarin and fluorescein probes. The quantitative result generated the order **6RCDNB** > **CCDNB** > **FCDNB**. A combination of quantitative and qualitative results brought forth the overall binding efficiencies of the probe toward the BL-tag technique. The final order was found to be **6RCDNB** > **CCDNB** > **FCDNB** > **5RCDNB**. This ordering is the overall effect of disaggregation followed by the elimination step in BL-tag technology, and both of them are dependent upon the aggregation interactions between fluorophores and DNB quenchers.

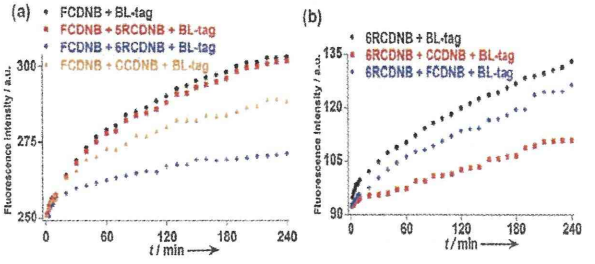

Fig. 5 (a) Time-dependent emission enhancement spectra (λ_{ex} = 497 nm and λ_{em} = 520 nm) of **FCDNB** (conc. of **FCDNB**: 1.0 μM) in presence of BL-tag with equimolar amounts of other probes in 100 mM HEPES buffer (pH 7.4) containing 0.1% DMSO at 25 °C. (b) Time-dependent emission enhancement spectra (λ_{ex} = 558 nm and λ_{em} = 575 nm) of **6RCDNB** (conc. of **6RCDNB**: 1.0 μM) in presence of BL-tag with equimolar amount of fluorescein and coumarin probes in 100 mM HEPES buffer (pH 7.4) containing 0.1% DMSO at 25 °C.

Protein labeling in living cells

In our present study, we used confocal microscopy for site-specific cell membrane labeling studies with the BL-tag fused with the N-terminus of the EGFR protein using fluorescein and coumarin fluorophore-based probes. We have chosen the probes according to their well-separated excitation wavelengths. HEK293T cells expressed with the BL-EGFR fusion protein were used for site-specific labeling of **CCDNB** and **FCDNB** (Fig. 6). Fluorescence images of the HEK293T cells were taken after probe treatment. Specific labeling of the cell membranes expressing the BL-EGFR fusion protein was observed with **CCDNB** (Fig. 6a). In the case of **FCDNB** (Fig. 6e), the cell membrane labeling was observed to be similar to that obtained in our previous experiment with an inverted fluorescence microscope.[13] On the other hand, in HEK293T cells expressed with the EGFR protein without any BL-tag, neither the coumarin- nor the fluorescein-labeled cell was observed (Fig. 6c and g).

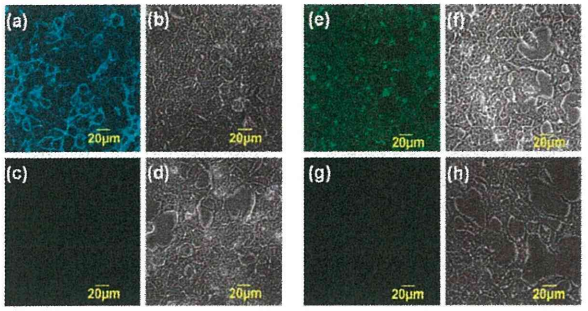

Fig. 6 Optical microscopic images of (a–d) **CCDNB** and (e–h) **FCDNB**-labeled HEK293T cells expressing (a,b,e,f) BL-EGFR and (c,d,g,h) EGFR. (a,c,e,g) Fluorescence microscopic images and (b,d,f,h) phase contrast microscopic images. For fluorescence microscopic images, the cells were excited by 405 nm and 473 nm laser lights for **CCDNB** and **FCDNB**, respectively.

Conclusions

In conclusion, we have developed a protein labeling method with comparative wide varieties of fluorophores involving a specific order for an aggregation and elimination-based BL-tag method. This technique is now established to be applicable without any restriction in the choice of the fluorophore, and more precisely, this technique has control over the reaction kinetics through the involved aggregation method. Based on appropriate demand of color for cell imaging, modification of the probe design is possible to get success in labeling of more than one targeted protein of interest. The color palette of this technique would help to combine this method with other methods known in the literature to tag different proteins in living cell simultaneously. Modification of the quencher part with more efficient quenched probes will help to obtain maximum fluorogenicity from this technique. We are now developing a method to reduce the incubation period in live cell imaging studies.

Experimental section

See supporting information for full experimental details and the labeling scheme of protons for assigning ^{1}H NMR of all the probes (Fig. S2 and S3) and other supporting materials, ESI.†

Synthesis of **CCDNB**. Compound **8** (Fig. S1, ESI†) (24 mg, 0.3 mmol) and 7-hydroxycoumarin-3-carboxylic acid *N*-succinimidyl ester (9 mg, 0.3 mmol) were dissolved in 0.5 mL of *N*,*N*-dimethylformamide. To this solution, TEA (3 mg, 0.3 mmol) was added at 0 °C (Scheme S1, ESI†). The reaction was continued for 6 h. The desired product **CCDNB** was isolated using preparative HPLC (10 mg, y. 34%). ^{1}H NMR (DMSO-d_6, 400 MHz) δ 1.72 (m, 2H, 2 × a), 1.88 (m, 2H, 2 × b), 3.39–3.57 (m, 22H, 1 × c, 1 × d, 2 × e, 2 × f, 4 × g, 8 × h, 2 × i, 2 × j), 4.08 (br, 1H, k), 5.07 (s, 1H, l), 5.18 (d, 1H, m), 5.48 (m, 1H, n), 6.81 (d, 1H, o), 6.88 (dd, 1H, p), 7.19 (d, 1H, q), 7.39 (d, 2H, 2 × r), 7.74 (d, 2H, 2 × s), 7.81 (d, 1H, t), 8.23 (dd, 1H, u), 8.41 (m, 1H, v), 8.77 (s, 1H, w), 8.83 (d, 1H, x), 8.96 (br, 1H, ya), 8.96 (m, 1H, yb), 11.09 (s, 1H, z); ^{13}C NMR (DMSO-d_6 100 MHz) δ 28.4 (a, b), 35.4 (e), 36.8 (i), 37.2 (f), 41.1 (j), 68.5 (m), 68.6 (n), 69.8 (c), 69.9 (g), 70.0 (h), 111.2, 115.3, 119.7, 122.2, 123.8, 125.5, 127.9, 129.7, 130.2, 132.0, 134.9, 139.5, 148.3, 148.5, 155.9, 156.6 (Ar), 163.7, 167.9, 168.1, 168.7, 169.4 (C=O); HRMS ($C_{43}H_{46}N_7O_{16}S_2$, FAB+); Found 980.2464; Calc., 980.2437.

Synthesis of **5RCDNB** and **6RCDNB**. Compound **8** (24 mg, 0.3 mmol) and 5(6)-carboxytetramethylrhodamine, succinimidyl ester (5(6)-TAMRA, SE) (16 mg, 0.3 mmol) were dissolved in 0.5 mL of *N*,*N*-dimethylformamide. To this solution, TEA (3 mg, 0.3 mmol) was added at 0 °C (Scheme S2, ESI†). The reaction was continued for 6 h. The desired products **5RCDNB** and **6RCDNB** were isolated using preparative HPLC.

5RCDNB (6.5 mg, y. 18%); ^{1}H NMR (DMSO-d_6, 400 MHz) δ 1.72 (t, 2H, 2 × a), 1.87 (t, 2H, 2 × b), 2.96 (s, 12H, c), 3.40–3.54 (m, 18H, 2 × d, 2 × e, 6 × f), 3.81–4.1 (m, 3H, 2 × j + h, i), 5.10 (s, 1H, w), 5.18 (d, 1H, l), 6.51–6.58 (br, 6H, m), 7.21 (d, 1H, n), 7.32 (d, 1H, p), 7.37 (d, 2H, 2 × o), 7.74 (d, 2H, 2 × q), 8.22 (d, 1H, r), 8.42 (d, 1H, t), 8.48 (s, 1H, s), 8.86 (s, 1H, u), 8.99–9.15 (br, 3H, 3 × v); ^{13}C NMR (DMSO-d_6 100 MHz) δ 28.3 (a, i), 29.4 (b), 31.2 (g), 36.7 (e), 41.2, 42.6, 44.4 (c, d, j), 60.3 (k, l), 68.3, 73.6 (f), 98.1 (m), 115.2 (n), 119.5, 119.8, 120.5, 121.9, 122.6, 123.6, 125.9, 126.6, 127.3, 127.7, 128.6, 129.6, 130.0, 131.1, 134.6, 148.4 (Ar), 164.6, 165.1, 165.5, 168.4, 169.4, 169.8 (C=O); HRMS ($C_{58}H_{62}N_9O_{16}S_2$, FAB+); Found 1204.3783; Calc., 1204.3750.

6RCDNB (5 mg, y. 14%); ^{1}H NMR (DMSO-d_6, 400 MHz) δ 1.71 (t, 2H, 2 × a), 1.86 (t, 2H, 2 × b), 2.95 (s, 12H, c), 3.40–3.54 (m, 18H, 2 × d, 2 × e, 6 × f), 3.81–3.89 (m, 3H, 2 × j + h), 4.06 (d, 1H, i), 5.00 (br, 1H, w), 5.12 (d, 1H, l), 6.51 (br, 6H, m), 7.21 (d, 1H, n), 7.37 (d, 2H, 2 × o), 7.66 (s, 1H, p), 7.74 (d, 2H, 2 × q), 8.08 (d, 1H, r), 8.15 (d, 1H, s), 8.25 (d, 1H, t), 8.85 (d, 1H, u), 8.99 (br, 3H, 3 × v); ^{13}C NMR (DMSO-d_6 100 MHz) δ 28.2 (a, i), 29.3 (b, g), 36.6 (e), 41.0 (c, d, j), 60.3 (k, l), 68.2, 69.6, 69.7, 69.8 (f), 97.9 (m), 115.1 (n), 121.3, 123.6, 127.4, 127.8, 128.5, 129.6, 130.0, 131.8, 134.6, 135.6, 139.6, 140.8, 144.3, 148.3, 152.5, 153.6 (Ar), 162.1, 163.6, 165.0, 165.5, 168.1, 169.5 (C=O); HRMS ($C_{58}H_{62}N_9O_{16}S_2$, FAB+); Found 1204.3729; Calc., 1204.3750.

Acknowledgements

This research is supported by the Japan Society for the Promotion of Science (JSPS) through its "Funding Program for World-Leading Innovative R&D on Science and Technology (FIRST Program)." This work was supported in part by the CREST funding program from the Japan Science and Technology Agency (JST); a Grant-in-Aid for Scientific Research from the Ministry of Education, Culture, Sports, Science and Technology (MEXT) of Japan; and a Grant-in-Aid from the Ministry of Health, Labour and Welfare (MHLW) of Japan. KKS and SW acknowledge support from a Global COE Fellowship of Osaka University. SW acknowledges a JSPS Research Fellowship.

Notes and references

1 (*a*) Z. Zhou, A. Koglin, Y. Wang, A. P. McMahon and C. T. Walsh, *J. Am. Chem. Soc.*, 2008, **130**, 9925–9930; (*b*) S. S. Gallagher, J. E. Sable, M. P. Sheetz and V. W. Cornish, *ACS Chem. Biol.*, 2009, **4**, 547–556; (*c*) R. McRae, P. Bagchi, S. Sumalekshmy and C. J. Fahrni, *Chem. Rev.*, 2009, **109**,

4780–4827; (*d*) H. Ren, F. Xiao, K. Zhan, Y.-P. Kim, H. Xie, Z. Xia and J. Rao, *Angew. Chem., Int. Ed.*, 2009, **48**, 9658–9662; (*e*) S. Mizukami, S. Watanabe, Y. Hori and K. Kikuchi, *J. Am. Chem. Soc.*, 2009, **131**, 5016–5017; (*f*) D. Maurel, S. Banala, T. Laroche and K. Johnsson, *ACS Chem. Biol.*, 2010, **5**, 507–516; (*g*) C. Uttamapinant, K. A. White, H. Baruah, S. Thompson, M. Fernández-Suárez, S. Puthenveetil and A. Y. Ting, *Proc. Natl. Acad. Sci. U. S. A.*, 2010, **107**, 10914–10919; (*h*) D. Srikun, A. E. Albers, C. I. Nam, A. T. Iavarone and C. J. Chang, *J. Am. Chem. Soc.*, 2010, **132**, 4455–4465.

2 (*a*) D. Summerer, S. Chen, N. Wu, A. Deiters, J. W. Chin and P. G. Schultz, *Proc. Natl. Acad. Sci. U. S. A.*, 2006, **103**, 9785–9789; (*b*) C. Smith, *Nature*, 2007, **4**, 755–759; (*c*) A. Olichon and T. Surrey, *J. Biol. Chem.*, 2007, **282**, 36314–36320; (*d*) W. Sandtner, F. Bezanilla and A. M. Correa, *Biophys. J.*, 2007, **93**, L45–L47; (*e*) J. Artus and A.-K. Hadjantonakis, in *Modern Research and Educational Topics in Microscopy*, ed. A. Mendez-Vilas and J. Diaz, Formatex, 2007, pp. 190–202; (*f*) M. Z. Lin and L. wang, *Physiology*, 2008, **23**, 131–141; (*g*) R. W. Watkins, L. D. Lavis, V. M. Kung, G. V. Los and R. T. Raines, *Org. Biomol. Chem.*, 2009, **7**, 3969–3975.

3 (*a*) B. A. Griffin, S. R. Adams and R. Y. Tsien, *Science*, 1998, **281**, 269–272; (*b*) B. A. Griffin, S. R. Adams, J. Jones and R. Y. Tsien, *Methods Enzymol.*, 2000, **327**, 565–578; (*c*) S. R. Adams, R. E. Campbell, L. A. Gross, B. R. Martin, G. K. Walkup, Y. Yao, J. Llopis and R. Y. Tsien, *J. Am. Chem. Soc.*, 2002, **124**, 6063–6076; (*d*) C. Hoffman, G. Gaietta, M. Bunemann, S. R. Adams, S. Oberdolff-Maass, B. Behr, J.-P. Vilardaga, R. Y. Tsien and M. H. Ellisman, *Nat. Methods*, 2005, **12**, 453–462; (*e*) O. Tour, S. R. Adams, R. A. Kerr, R. M. Meijer, T. J. Sejnowski, R. W. Tsien and R. Y. Tsien, *Nat. Chem. Biol.*, 2007, **3**, 423–431; (*f*) S. R. Adams and R. Y. Tsien, *Nat. Protoc.*, 2008, **3**, 1527–1534.

4 (*a*) G. V. Los, A. Darzins, N. Karassina, C. Zimprich, R. Learish, M. G. McDougall, L. P. Encell, R. Friedman-Ohana, M. Wood, G. Vidugiris, K. Zimmerman, P. Otto, D. H. Klaubert and K. V. Wood, *Cell Notes*, 2005, **11**, 2–6; (*b*) G. V. Los, L. P. Encell, M. G. McDougall, D. D. Hartzell, N. Karassina, C. Zimprich, M. G. Wood, R. Learish, R. F. Ohana, M. Urh, D. Simpson, J. Mendez, K. Zimmerman, P. Otto, G. Vidugiris, J. Zhu, A. Darzins, D. H. Klaubert, R. F. Bulleit and K. V. Wood, *ACS Chem. Biol.*, 2008, **3**, 373–382; (*c*) J. Schroder, H. Benink, M. Dyba and G. V. Los, *Biophys. J.*, 2009, **96**, L01–L03; (*d*) R. F. Ohana, L. P. Encell, K. Zhao, D. Simpson, M. R. Slater, M. Urh and K. V. Wood, *Protein Expression Purif.*, 2009, **68**, 110–120.

5 (*a*) A. Keppler, S. Gendreizig, T. Gronemeyer, H. Pick, H. Vogel and K. Johnsson, *Nat. Biotechnol.*, 2003, **21**, 86–89; (*b*) A. Keppler, H. Pick, C. Arrivoli, H. Vogel and K. Johnsson, *Proc. Natl. Acad. Sci. U. S. A.*, 2004, **101**, 9955–9959; (*c*) M. Kindermann, I. Sielaff and K. Johnsson, *Bioorg. Med. Chem. Lett.*, 2004, **14**, 2725–2728; (*d*) N. Johnsson and K. Johnsson, *ACS Chem. Biol.*, 2007, **2**, 31–38; (*e*) A. Gautier, A. Juilleratk, C. Heinis, I. R. Corrêa Jr., M. Kindermann, F. Beaufils and K. Johnsson, *Chem. Biol.*, 2008, **15**, 128–136; (*f*) M. Bannwarth, I. R. Corrêa Jr., M. Sztretye, S. Pouvreau, C. Fellay, A. Aebischer, L. Royer, E. Ríos and K. Johnsson, *ACS Chem. Biol.*, 2009, **4**, 179–190; (*g*) M. A. Brun, K.-T. Tan, E. Nakata, M. J. Hinner and K. Johnsson, *J. Am. Chem. Soc.*, 2009, **131**, 5873–5884.

6 (*a*) A. Ojida, K. Honda, D. Shinmi, S. Kiyonaka, Y. Mori and I. Hamachi, *J. Am. Chem. Soc.*, 2006, **128**, 10452–10459; (*b*) H. Nonaka, S. Tsukiji, A. Ojida and I. Hamachi, *J. Am. Chem. Soc.*, 2007, **129**, 15777–15779.

7 Y. Sekine-Aizawa and R. L. Huganir, *Proc. Natl. Acad. Sci. U. S. A.*, 2004, **101**, 17114–17119.

8 T. L. Halo, J. Appelbaum, E. M. Hobert, D. M. Balkin and A. Schepartz, *J. Am. Chem. Soc.*, 2009, **131**, 438–439.

9 (*a*) L. W. Miller, J. Sable, P. Goelet, M. P. Sheetz and V. W. Cornish, *Angew. Chem., Int. Ed.*, 2004, **43**, 1672–1675; (*b*) L. W. Miller, Y. Cai, M. P. Sheetz and V. W. Cornish, *Nat. Methods*, 2005, **2**, 255–257; (*c*) N. T. Calloway, M. Choob, A. Sanz, M. P. Sheetz, L. W. Miller and V. W. Cornish, *ChemBioChem*, 2007, **8**, 767–774; (*d*) S. S. Gallagher, J. E. Sable, M. P. Sheetz and V. W. Cornish, *ACS Chem. Biol.*, 2009, **4**, 547–556; (*e*) H. E. Rajasekhar, D. R. Reddy, S. Mohandessi, N. G. Butlin and L. W. Miller, *Angew. Chem., Int. Ed.*, 2009, **48**, 4990–4992.

10 C. Szent-Gyorgyi, B. F. Schmidt, Y. Creeger, G. W. Fisher, K. L. Zakel, S. Adler, J. A. Fitzpatrick, C. A. Woolford, Q. Yan, K. V. Vasilev, P. B. Berget, M. P. Bruchez, J. W. Jarvik and A. Waggoner, *Nat. Biotechnol.*, 2008, **26**, 235–240.

11 S. Watanabe, S. Mizukami, Y. Hori and K. Kikuchi, *Bioconjugate Chem.*, 2010, **21**, 2320–2326.

12 (*a*) D. Maurel, L. Comps-Agrar, C. Brock, M.-L. Rives, E. Bourrier, M. A. Ayoub, H. Bazin, N. Tinel, T. Durroux, L. Prézeau, E. Trinquet and J.-P. Pin, *Nat. Methods*, 2008, **5**, 561–567; (*b*) F. Kampmeier, M. Ribbert, T. Nachreiner, S. Dembski, F. Beaufils, A. Brecht and S. Barth, *Bioconjugate Chem.*, 2009, **20**, 1010–1015.

13 K. K. Sadhu, S. Mizukami, S. Watanabe and K. Kikuchi, *Chem. Commun.*, 2010, **46**, 7403–7405.

14 (*a*) G. Guillaume, M. Vanhove, J. Lamotte-Brasseur, P. Ledent, M. Jamin, B. Joris and J.-M. Frère, *J. Biol. Chem.*, 1997, **272**, 5438–5444; (*b*) H. Adachi, T. Ohta and H. Matsuzawa, *J. Biol. Chem.*, 1991, **266**, 3186–3191.

15 G. Punte and B. E. Rivero, *Acta Crystallogr., Sect. C: Cryst. Struct. Commun.*, 1989, **45**, 1952–1957.

16 K. Kumar and P. R. Carey, *J. Chem. Phys.*, 1975, **63**, 3697–3707.

17 (*a*) E. L. Kapinus and I. I. Dilung, *Chem. Phys. Lett.*, 1990, **174**, 75–79; (*b*) U. Wenzel and H.-G. Lohmannsroben, *J. Photochem. Photobiol., A*, 1996, **96**, 13–18; (*c*) S. Santabarbara, R. Barbato, G. Zucchelli, F. M. Garlaschi and R. S. Jennings, *FEBS Lett.*, 2001, **505**, 159–162; (*d*) K.-S. Focsaneanu and J. C. Scaiano, *Photochem. Photobiol. Sci.*, 2005, **4**, 817–821; (*e*) H. Li, J. Kang, L. Ding, F. Lu and Y. Fang, *J. Photochem. Photobiol., A*, 2008, **197**, 226–231.

18 Y. Oseki, M. Fujitsuka, D. W. Cho, A. Sugimoto, S. Tojo and T. Majima, *J. Phys. Chem. B*, 2005, **109**, 19257–19262.

19 (*a*) R. Livingston, L. Thompson and M. V. Ramarao, *J. Am. Chem. Soc.*, 1952, **74**, 1073–1075; (*b*) J. C. Nnadi, A. W. Peters and S. Y. Wang, *J. Am. Chem. Soc.*, 1972, **94**, 712–716; (*c*) M. Sirish and B. G. Maiya, *J. Photochem. Photobiol., A*, 1994, **77**, 189–200; (*d*) E. Tyystjärvi, N. King, M. Hakala and E.-M. Aro, *J. Photochem. Photobiol., B*, 1999, **48**, 142–147; (*e*) C. Zhang, *J. Phys. Chem. A*, 2006, **110**, 14029–14035.

20 S. Vijayakumar, G. Ravishanker, R. F. Pratt and D. L. Beveridge, *J. Am. Chem. Soc.*, 1995, **117**, 1722–1730.

JACS
JOURNAL OF THE AMERICAN CHEMICAL SOCIETY

ARTICLE

pubs.acs.org/JACS

In Vivo Fluorescence Imaging of Bone-Resorbing Osteoclasts

Toshiyuki Kowada,[†] Junichi Kikuta,[‡,§] Atsuko Kubo,[‡,§] Masaru Ishii,[‡,§] Hiroki Maeda,[¶] Shin Mizukami,[†,¶] and Kazuya Kikuchi*[,†,¶]

[†]Laboratory of Chemical Imaging Techniques, Immunology Frontier Research Center (IFReC), Osaka University, Osaka, Japan
[‡]Laboratory of Cellular Dynamics, Immunology Frontier Research Center (IFReC), Osaka University, Osaka, Japan
[§]Japan Science and Technology Agency (JST), CREST, Tokyo, Japan
[¶]Department of Material and Life Science, Graduate School of Engineering, Osaka University, Osaka, Japan

Supporting Information

ABSTRACT: Osteoclasts are giant polykaryons responsible for bone resorption. Because an enhancement or loss of osteoclast function leads to bone diseases such as osteoporosis and osteopetrosis, real-time imaging of osteoclast activity in vivo can be of great help for the evaluation of drugs. Herein, pH-activatable chemical probes BAp-M and BAp-E have been developed for the detection of bone-resorbing osteoclasts in vivo. Their acid dissociation constants (pK_a) were determined as 4.5 and 6.2 by fluorometry in various pH solutions. These pK_a values should be appropriate to perform selective imaging of bone-resorbing osteoclasts, because synthesized probes cannot fluoresce intrinsically at physiological pH and the pH in the resorption pit is lowered to about 4.5. Furthermore, BAp-M and BAp-E have a bisphosphonate moiety that enabled the probes to localize on bone tissues. The hydroxyapatite (HA) binding assay in vitro was, therefore, performed to confirm the tight binding of the probes to the bone tissues. Our probes showed intense fluorescence at low pH values but no fluorescence signal under physiological pH conditions on HA. Finally, we applied the probes to in vivo imaging of osteoclasts by using intravital two-photon microscopy. As expected, the fluorescence signals of the probes were locally observed between the osteoclasts and bone tissues, that is, in resorption pits. These results indicate that our pH-activatable probes will prove to be a powerful tool for the selective detection of bone-resorbing osteoclasts in vivo, because this is the first instance where in vivo imaging has been conducted in a low-pH region created by bone-resorbing osteoclasts.

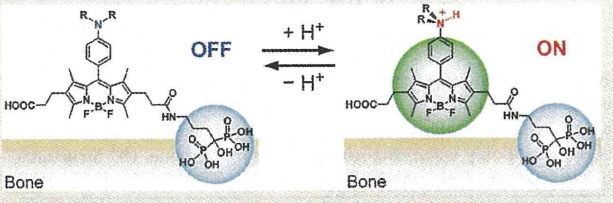

INTRODUCTION

Osteoclasts are giant multinucleated cells derived from monocytoid hematopoietic cells, which are responsible for bone resorption within the bone-remodeling compartment.[1−4] Because an enhancement or loss of osteoclast function causes bone diseases such as osteoporosis or osteopetrosis, real-time imaging of osteoclast activity in vivo is one of the most important tools required for investigations of osteoclast functions.[4] However, current bone imaging techniques such as computed tomography (CT) and biochemical markers of bone metabolism cannot connect spatial information with cellular activity. To overcome this problem, fluorescence imaging is a promising technique for obtaining temporal and spatial information about target cells or proteins.[5] Thus, we sought to develop fluorescent chemical probes with an OFF/ON switch, which can selectively detect active osteoclasts and thereby instantaneously provide an image of the location of the osteoclasts activated by particular stimuli. Furthermore, two-photon excitation microscopy can provide noninvasive imaging of osteoclasts in vivo.[6]

Active osteoclasts resorb the organic and inorganic components of the bone tissues by cathepsin K secretion and by proton extrusion, which causes acidification of the bone surface.[4] To the best of our knowledge, there have been no reports on the detection of protons extruded by osteoclasts. Only a single report has demonstrated the indirect in vivo detection of cathepsin K activity.[7] However, the cathepsin K probe has not yet provided real-time imaging data about the osteoclasts in the process of resorbing bone tissues, and its selectivity as a probe for the detection of osteoclast formation is inadequate.

We recognized that active osteoclasts can be selectively detected through specific imaging of low-pH regions by using a pH-activatable fluorescent probe[8] with specific delivery of the probe using a bisphosphonate group[9] (Figure 1a). In addition, this probe should be quite useful in the evaluation of drugs.

There are two requirements for the development of new probes for selective detection of bone-resorbing osteoclasts. One obvious requirement is a pH-sensitive fluorescence switch, and the other is the capability to localize on the bone tissue. Therefore, we designed fluorescent probes called "BAps". These probes are composed of boron−dipyrromethene (BODIPY) dye and a bisphosphonate group (Figure 1b). BODIPY dyes are

Received: July 12, 2011
Published: September 22, 2011

dx.doi.org/10.1021/ja2064582 | J. Am. Chem. Soc. 2011, 133, 17772–17776

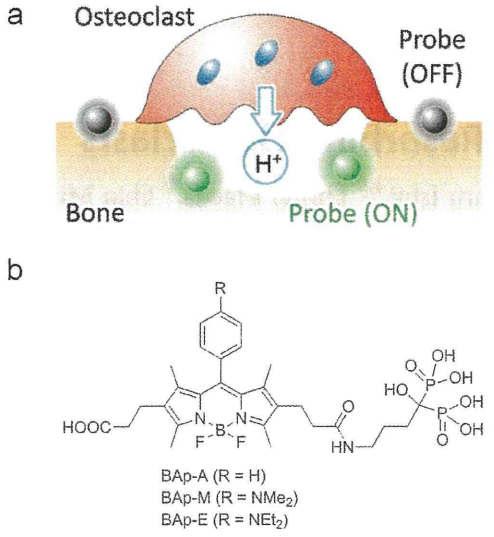

Figure 1. Strategy for selective detection of bone-resorbing osteoclasts using pH-activatable probes and design of BAps. (a) pH-activatable probes are immobilized on the bone tissue and provide intense fluorescence only when osteoclasts are resorbing bone. (b) Structures of the pH-activatable probes (BAps).

well-known fluorophores that have been used in a large number of applications because of their environmental stability, large molar absorption coefficients, and high fluorescence quantum yields.[10] Most recently, pH-activatable fluorescence probes including a BODIPY dye have been developed for the detection of cancers and real-time monitoring of therapy.[11] Furthermore, bisphosphonate compounds are currently used as drugs for the treatment of various bone diseases. These compounds chelate calcium and inhibit bone resorption. We, therefore, decided to combine a BODIPY-based pH-sensing unit with a bisphosphonate compound.

RESULTS AND DISCUSSION

Characterization of BAps. To demineralize the bone matrix, osteoclasts secrete protons (H^+) into the resorption pit where the pH value is lowered to about 4.5.[3] We, therefore, considered that selective imaging of osteoclasts would be achieved by the development of pH-activatable probes with an acid dissociation constant (pK_a) in the range of 4.5−6.5, because those probes cannot intrinsically fluoresce at the physiological pH. According to this assumption, we designed and synthesized three fluorescent probes with different pK_a values (Figure 1b). A control probe with "always-ON" fluorescence (BAp-A) was developed. The other probes are fluorescence "turn-ON" type sensors that can detect the acidic pH environment. Since the fluorescence OFF/ON switching mechanism is based on photoinduced electron transfer (PeT), the pK_a values of these probes can be finely tuned by the appropriate choice of an electron-donating moiety attached to the BODIPY core.[12] Thus, we chose *p*-dimethylanilino (BAp-M) and *p*-diethylanilino groups (BAp-E) as the electron-donating moieties to provide pK_a values in the range of 4.5−6.5.

The fluorescent probes were synthesized in one step from the corresponding dicarboxylic acids by using straightforward synthetic pathways (Scheme S1, Supporting Information). To confirm the pH-dependent fluorescence properties of BAps, we

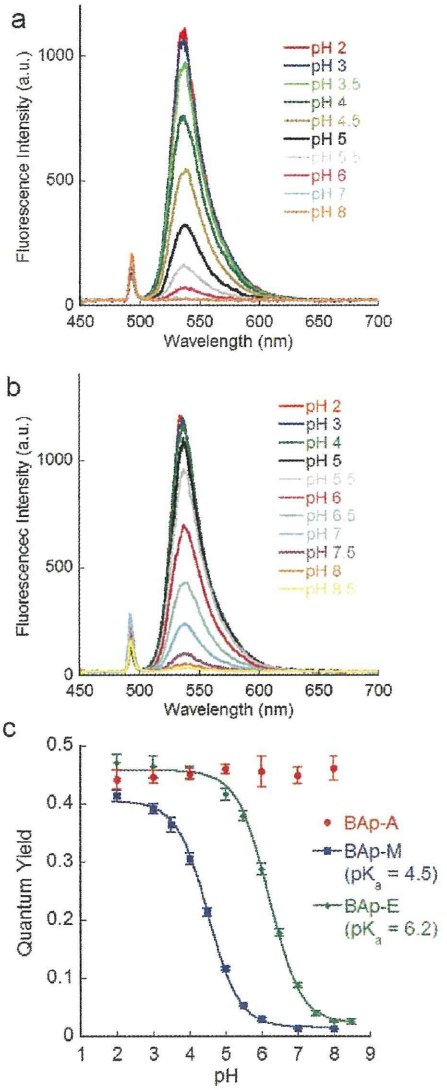

Figure 2. Fluorescence spectra (0.2 μM, excited at 492 nm) of (a) BAp-M and (b) BAp-E in citrate-phosphate buffer, and (c) pH-dependent profiles of changes in fluorescence quantum yield of BAps. The data were fitted to the Henderson−Hasselbalch equation.

measured the absorption and emission spectra in citrate-phosphate buffer at different pH values (Figures S1 and 2). All three probes had absorption maxima at about 520 nm. These peaks were found to be independent of the pH of the buffer. These results indicate that any structural changes or aggregations of the dye induced by pH changes do not occur in aqueous solution. In contrast, the fluorescence intensities of BAp-M and BAp-E were highly affected by the pH (Figure 2). The fluorescence intensities of BAp-M and BAp-E decreased along with an increase in pH. Essentially, no fluorescence was observed at the physiological pH. This phenomenon can be rationalized by the observation that PeT actually occurs from the *p*-anilino group to the BODIPY core.[12] Thus, these two probes showed a fluorescence "turn-ON" type increase at lower pH. Furthermore, the pK_a values were estimated by fitting pH-dependent changes of the fluorescence quantum yield to the

dx.doi.org/10.1021/ja2064582 |J. Am. Chem. Soc. 2011, 133, 17772–17776

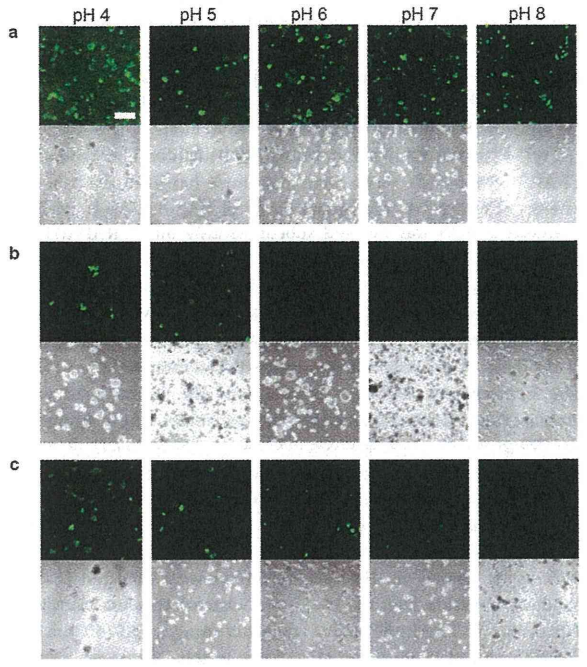

Figure 3. Confocal microscope images of BAps binding to hydroxyapatite in McIlvaine's citrate-phosphate buffer. Scale bar: 40 μm. (a) BAp-A. (b) BAp-M. (c) BAp-E.

Henderson–Hasselbalch equation (Figure 2c). Consequently, the pK_a values of BAp-M and BAp-E were 4.5 and 6.2, respectively. These results indicate that the two pH-activatable probes could be used to selectively visualize the bone-resorbing osteoclasts. On the other hand, BAp-A showed intense fluorescence regardless of pH changes as would be expected by an "always-ON" fluorescence probe.

Hydroxyapatite Binding Test. Bone tissues are mainly composed of type I collagen and hydroxyapatite (HA). Confocal microscopy was then performed to ascertain the HA binding activity and the fluorescence properties of BAps bound to HA. Intense fluorescence was observed from every HA particle, which was mixed with BAp-A and soaked in buffer at different pH values (Figure 3). We next examined the pH-activatable probes, namely, BAp-M and BAp-E. In the case of BAp-M, the fluorescence signals from HA particles were hardly observed under physiological conditions, i.e., at pH 7.0 and pH 8.0. The fluorescence intensities gradually increased with the decrease in the pH value, and consequently, intense fluorescence was observed below pH 5.0. Similar to the behavior in solution, the HA particle including BAp-E responded in an environment of higher pH relative to BAp-M, and showed intense fluorescence. However, the fluorescence signals were very weak or not observed at pH 7.0 or 8.0. These results indicate that BAps are pH-sensitive not only in aqueous solution but also in the solid state, when bound to HA. It was thus expected that synthesized probes could be immobilized on bone tissue and that they will retain their pH-sensitive properties in vivo.

In Vivo Imaging of Osteoclasts. To clarify the osteoclast function and develop new therapeutic agents to treat bone diseases, real-time monitoring of living osteoclasts in vivo will be very important. However, it is challenging to observe living osteoclasts that are present in the medullary cavity, deep inside the bone.

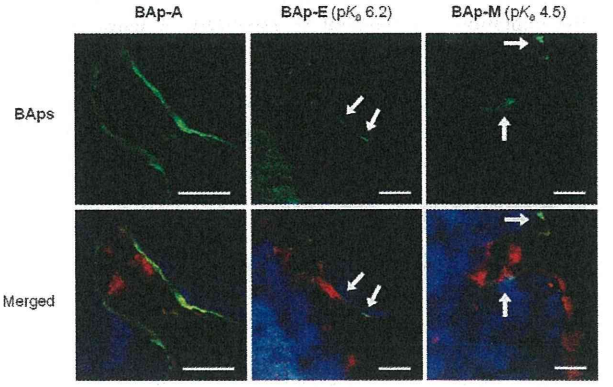

Figure 4. Two-photon excitation microscopy images of in vivo osteoclasts using BAps. PBS solution of BAps (green) was subcutaneously administered daily for 3 days to TRAP-tdTomato (red) transgenic mice. Second harmonic generation from collagen in the bone matrix is presented as a blue signal. Scale bars: 40 μm.

We used two-photon excitation microscopy, which can penetrate deeply into tissues, to capture images of osteoclasts through the parietal bone of mice.[6] The parietal bone is relatively thin, and the distance between the bone surface and the medullary cavity is 80–120 μm. This allowed us to achieve real-time imaging of the active osteoclasts in vivo. To ensure that BAps can function in a living mouse, we administered the probes to mice and evaluated their pH-sensitive properties by the above-described method (Figure 4). The blue signal indicates second harmonic generation from collagen fibers in the bone matrix. It is obvious that osteoclasts were present in the medullary cavity, because we used TRAP (tartrate-resistant acid phosphatase)-tdTomato transgenic mice, in which TRAP-positive mature osteoclasts predominantly express tdTomato.[13] To confirm whether the synthesized probes can be transported and immobilized on the bone tissues, we first used the "always-ON" probe BAp-A (Figure 4). As expected, green fluorescence was observed all over the bone surface. We next examined in vivo imaging of osteoclasts by using pH-activatable probes. In contrast to the case of BAp-A, green signals were locally observed only between the osteoclasts and the bone tissues (Figure 4, white arrow). Although the green staining was also observed in the lower left of the BAp-E panels, it is mainly derived from second harmonic generation from the bone matrix (Figure S2, Supporting Information). These results indicate that our probes are functioning properly, and have the potential to detect the bone-resorbing osteoclasts in vivo. Moreover, it is expected that the pH value in the resorption pit created by an osteoclast should be within the range of 4–6, because more intense fluorescence is found using BAp-E, which has a higher pK_a value relative to BAp-M. The brightness of BAp-E ($\varepsilon_{abs,450} \times \Phi$) between pH 4 and pH 6 is roughly 1.2–7.5 times as intense as that of BAp-M. Until now, the pH value in the resorption pit had not been measured in vivo. Therefore, we expect that this method will be helpful to estimate the pH value in the resorption pits.

CONCLUSION

We demonstrated that our custom-designed probes, in particular, BAp-E, fluoresce in the low-pH environment created by osteoclasts in vivo, as well as in a cuvette. From medicinal and

therapeutic points of view, an imaging technique for visualizing the migration and function of osteoclasts is highly desirable. Because this method is the first example of in vivo imaging of a low-pH region created by bone-resorbing osteoclasts, we are confident that the pH-activatable probes BAps will provide a powerful tool for the selective detection of bone-resorbing osteoclasts in vivo.

EXPERIMENTAL SECTION

Synthesis of BAp-A. To a solution of the corresponding bis-carboxylic acid (1,3,5,7-tetramethyl-2,6-bis(2-carboxyethyl)-8-phenyl-4,4-difluoro-4-bora-3a,4a-diaza-*s*-indacene)[11] (9.40 mg, 20.1 μmol) in MeCN (5 mL) were added alendronic acid (5.00 mg, 20.1 μmol) in water (4 mL), 2 N aq NaOH (60 μL, 120 μmol), and DMT-MM (27.7 mg, 100 μmol) at room temperature. After being stirred for 16 h, the reaction mixture was poured into 10% aqueous solution of AcOH (11 mL) and lyophilized. The crude compound was then purified by reverse-phase HPLC under the following conditions: A/B = 85/15 (0 min) to 10/90 (30 min) (solvent A: 100 mM aq TEAA; solvent B: acetonitrile). Compound eluted with a retention time of 12 min was collected. After lyophilization, a orange powder of BAp-A·3Et$_3$N was obtained (6.55 mg, 6.53 μmol) in 32% yield. ^{1}H NMR (400 MHz, D_2O) δ 0.95 (s, 3H), 0.97 (s, 3H), 1.12 (t, J = 7.2 Hz, 27H), 1.64−1.67 (m, 2H), 1.75−1.85 (m, 2H), 2.01−2.09 (m, 4H), 2.25−2.37 (m, 10H), 3.00−3.07 (m, 20H), 6.71 (br s, 2H), 7.14 (br s, 3H). HRMS (FAB−) Calcd for $[M - H^+]^-$ 698.2021, found 698.2010.

Synthesis of BAp-M. BAp-M was synthesized from the corresponding bis-carboxylic acid (1,3,5,7-tetramethyl-2,6-bis(2-carboxyethyl)-8-(*p*-dimethylaminophenyl-4,4-difluoro-4-bora-3a,4a-diaza-*s*-indacene)[11] by the same method as described above and purified by reverse-phase HPLC under the following conditions: A/B = 75/25 (0 min) to 60/40 (20 min), and then 10/90 (25 min) (solvent A: 100 mM aq TEAA; solvent B: acetonitrile). A orange powder of BAp-M·3Et$_3$N (t_R = 11 min) was obtained in 9% yield. ^{1}H NMR (400 MHz, D_2O) δ 1.10−1.14 (m, 33H), 1.63 (br s, 2H), 1.78 (br s, 2H), 2.02−2.10 (m, 4H), 2.28 (s, 3H), 2.32 (s, 3H), 2.41 (br s, 4H), 2.74 (s, 6H), 2.97−3.06 (m, 20H), 6.71 (br s, 4H). HRMS (FAB−) Calcd for $[M - H^+]^-$ 741.2443, found 741.2462.

Synthesis of BAp-E. BAp-E was synthesized from the corresponding bis-carboxylic acid (1,3,5,7-tetramethyl-2,6-bis(2-carboxyethyl)-8-(*p*-diethylaminophenyl-4,4-difluoro-4-bora-3a,4a-diaza-*s*-indacene)[11] by the same method as described above and purified by reverse-phase HPLC under the following conditions: A/B = 80/20 (0 min) to 10/90 (30 min) (solvent A: 100 mM aq TEAA; solvent B: acetonitrile). A orange powder of BAp-E·3Et$_3$N (t_R = 13 min) was obtained in 11% yield. ^{1}H NMR (400 MHz, D_2O) δ 0.95 (t, J = 7.2 Hz, 6H), 1.08 (s, 3H), 1.13 (t, J = 7.2 Hz, 27H), 1.18 (s, 3H), 1.60−1.65 (m, 2H), 1.71−1.83 (m, 2H), 2.03−2.11 (m, 4H), 2.28 (s, 3H), 2.35 (s, 3H), 2.40−2.46 (m, 4H), 2.93−2.98 (m, 2H), 3.05 (q, J = 7.2 Hz, 18H), 3.34 (q, J = 7.2 Hz, 4H), 6.93 (d, J = 8.0 Hz, 2H), 7.07 (d, J = 8.4 Hz, 2H). HRMS (FAB−) Calcd for $[M - H^+]^-$ 769.2756, found 769.2743.

High-Performance Liquid Chromatography. We performed HPLC on a system composed of a pump (PU-2080, JASCO) and a detector (MD-2010, JASCO) with an Inertsil ODS-3 (4.6 mm × 250 mm for analysis; 10.0 mm × 250 mm for preparation).

Fluorometry. Fluorescence spectra were measured in McIlvaine's citrate-phosphate buffer using a Hitachi F4500 spectrometer. Slit width was 2.5 nm for both excitation and emission, and the photomultiplier voltage was 950 V. Fluorescence quantum yields were determined using fluorescein in 0.1 N NaOH as a standard (Φ = 0.85, λ_{ex} = 492 nm).

In Vitro Hydroxyapatite Binding Test. Five milligrams/mL of hydroxyapatite was vortexed in a 1 μM aqueous solution of BAps (1 mL) for 30 min at room temperature. The mixture was centrifuged and washed four times with water. A portion of the residual powder was soaked in citrate-phosphate buffer (400 μL) at various pH values in a glass-bottom dish. Fluorescence images were then collected using a confocal laser scanning microscope (Olympus, FLUOVIEW FV10i) equipped with a 60× lens. The excitation wavelength was 473 nm, and the emission was filtered with a BA490−590 filter.

Two-Photon Excitation Imaging in Mice. The generation of TRAP promoter-tdTomato transgenic mice has been described elsewhere.[13] Twenty-five micrograms/body of BAp-A, BAp-E, or BAp-M dissolved in PBS was injected subcutaneously into TRAP-tdTomato mice once a day beginning 3 days prior to the recording of images. Intravital microscopy of mouse calvaria bone tissues was performed using a protocol modified from a previous study.[6] Mice were anesthetized with isoflurane (Escain; 2% vaporized in 100% oxygen), and the hair at the neck and scalp was removed with hair removal lotion (Kracie). The frontoparietal skull was exposed, and the mouse head was immobilized in a custom-designed stereotactic holder. The imaging system was composed of a multiphoton microscope (SP5; Leica) driven by a laser (Mai-Tai HP Ti: Sapphire; Spectraphysics) tuned to 900 nm and an upright microscope (DM6000B; Leica) equipped with a 20× water immersion objective (HCX APO, N.A. 1.0; Leica). The microscope was enclosed in an environmental chamber in which anesthetized mice were warmed by heated air. Fluorescent probes were detected through a bandpass emission filter at 525/50 nm. Osteoclasts were visualized by expression of TRAP-tdTomato (detected using a 585/40 nm filter). Snapshot images were acquired, and raw imaging data were processed with Imaris (Bitplane) with a Gaussian filter for noise reduction. In vivo imaging experiments were performed three times for each probe, and representative images are shown.

ASSOCIATED CONTENT

Supporting Information. Synthetic scheme, photophysical properties, and high-performance liquid chromatograms of BAps, and images of negative control experiment in vivo. This material is available free of charge via the Internet at http://pubs.acs.org.

AUTHOR INFORMATION

Corresponding Author
kkikuchi@mls.eng.osaka-u.ac.jp

ACKNOWLEDGMENT

This work was partially supported by the Japan Society for the Promotion of Science (JSPS) through its "Funding Program for World-Leading Innovative R&D on Science and Technology (FIRST) Program" and by the Ministry of Education, Culture, Sports, Science and Technology (MEXT) of Japan (Grant No. 22108519 and 20675004). K.K. and M.I. express their special thanks for support from the Takeda Science Foundation and the Mochida Memorial Foundation. K.K. also thanks the Naito Foundation for financial support. K.K. and S.M. acknowledge the Asahi Glass Foundation for financial support.

REFERENCES

(1) Boyle, W. J.; Simonet, W. S.; Lacey, D. L. *Nature* **2003**, *423*, 337–342.
(2) Raggatt, L. J.; Partridge, N. C. *J. Biol. Chem.* **2010**, *285*, 25103–25108.
(3) Teitelbaum, S. L. *Science* **2000**, *289*, 1504–1508.
(4) Rodan, G. A.; Martin, T. J. *Science* **2000**, *289*, 1508–1514.